

Research papers

Urbanization enhances channel and surface runoff: A quantitative analysis using both physical and empirical models over the Yangtze River basin



Shuzhe Huang ^a, Yuan Gan ^a, Nengcheng Chen ^{a,b,c,*}, Chao Wang ^{a,*}, Xiang Zhang ^b, Chuxuan Li ^d, Daniel E. Horton ^d

^a State Key Laboratory of Information Engineering in Surveying, Mapping and Remote Sensing (LIESMARS), Wuhan University, Wuhan 430079, China

^b National Engineering Research Center of Geographic Information System, School of Geography and Information Engineering, China University of Geosciences (Wuhan), Wuhan, 430074, China

^c Hubei Luojia Laboratory, Wuhan 430079, China

^d Department of Earth and Planetary Sciences, Northwestern University, Evanston, IL, 60208, United States

ARTICLE INFO

ABSTRACT

Keywords:

Urbanization effect
Channel runoff
Surface runoff
Local climate zone
Hydrological model

Urbanization has become an irreversible trend and is even more rapid in flood-prone area. However, the responses of both channel runoff and surface runoff to the urbanization and the underlying mechanisms still deserve more in-depth exploration within urban extents with limited data availability. Accordingly, we conducted a comprehensive quantitative analysis of the urbanization effects on channel and surface runoff from both statistical and model-based perspectives over three major urban agglomerations (i.e., Chengyu (CY), middle region of Yangtze River (MYR), Yangtze River Delta (YRD)) in the Yangtze River Basin. The long-term high-resolution channel and surface runoff under different urbanization scenarios were simulated using both WRF-Hydro and SCS-CN models by integrating multiple remotely sensed, reanalysis, and in-situ datasets. Results demonstrated that the channel runoff increased by 4.4%, 5%, and 12.08% in CY, MYR, and YRD urban agglomerations, respectively. Meanwhile, the urbanization also contributed to 30%, 21.4%, and 17.7% of the surface runoff changes in three urban agglomerations. Based on the high-resolution local climate zone (LCZ), our results highlighted that the high-rise and middle-rise buildings and compact-arranged regions were more prone to accumulating surface runoff and trigger flooding events due to the weaker infiltration capacity of land surface with the densely distribution of impervious surface. Further machine learning based investigation and case analysis also explored the potential influencing factors and mechanisms of the impact of urbanization on channel and surface runoff. Results in the current research show further evidence that policy makers of urban planning and management need to consider and ensure societal preparedness for extreme runoff and flooding events.

1. Introduction

In recent decades, urbanization has emerged as a worldwide phenomenon characterized by the continuous increase in population density and the expansion of urban areas (Sun et al., 2020). Urban area was projected to increase by 1.2 million km² by 2030, almost the triple of the global urban area in 2000 (Seto et al., 2012). The rapid urbanization profoundly influences the water balance and energy exchange of the land-atmosphere system by altering the surface characteristics (e.g., the increasing impervious surface area and reduction of vegetation cover) in urban regions, leading to modifications in the local hydrological cycle and climate system (Huang et al., 2023a; Wang et al., 2023; Singh et al.,

2020). Numerous efforts have been dedicated to obtain more in-depth knowledge about the urbanization effects on hydrological responses (Huang et al., 2022a; Yu et al., 2022; Shen et al., 2023; Yang et al., 2019). In general, studies have demonstrated that urbanization induces a warmer environment in urban areas than the surrounding rural regions, namely urban heat island (UHI; Sun et al., 2014; Kong et al., 2020). Meanwhile, the frequency and intensity of extreme rainfall events are also found to increase in most cities around the world (Wang et al., 2021; Kishtawal et al., 2010; Guerreiro et al., 2018). Consequently, the spatio-temporal patterns of urban runoff undergo inevitable modifications due to the rapid urban expansion (Du et al., 2012; Miller and Hess, 2017). The urbanization process can impose great impacts on

* Corresponding authors.

E-mail addresses: cnc@whu.edu.cn (N. Chen), c.wang@whu.edu.cn (C. Wang).

the urban hydrological cycle and surface/underground flows through the expansion of impervious surface, modification of the natural drainage network, and degradation of the vegetation cover (Xu et al., 2018; Wu et al., 2022; Bibi et al., 2023; Zhang et al., 2022). These changes weaken soil infiltration capability, resulting in higher peak flows even under low-intensity and short-duration rainfall events (Zhang et al., 2018a; Chen et al., 2017). Previous research has also demonstrated the increased risk of flood hazard in urban regions due to the alteration of natural drainage network and the replacement of natural ecosystem (Kubal et al., 2009; Liu et al., 2022).

To address the escalating flood hazard, numerous studies have investigated the potential mechanisms of urbanization effects on urban runoff (Liu et al., 2021a; Biggs et al., 2022; Ramezani et al., 2023). Some research adopted observational runoff data from in-situ hydrological stations and applied statistical methods (e.g., trend detection algorithms, principle component analysis, and correlation analysis) to investigate the urbanization effects from a qualitative perspective (Walker et al., 2020; Westra et al., 2007). While these studies have revealed associations between increased runoff and urbanization, limitations persist due to data availability and methodology constraints. Generally, the studies over large river basins and urban environment have different needs of the applied datasets (Berezowski et al., 2012). Specifically, large river basins are usually treated as one unit for the hydrological calculation and analysis (Anand et al., 2018). In contrary, urban regions have more complicated land cover and hydrological conditions (e.g., buildings, artificial drainage network), which require finer and more additional inputs for accurate analysis of urban runoff (Huang et al., 2022b; Li et al., 2018). In this case, the remotely sensed gridded products with fine spatial resolution have the potential in providing detailed simulations of runoff in complex urban landscapes. (Huang et al., 2023b; Liu et al., 2021b; Debbage and Shepherd, 2019; Zhang et al., 2018b). Despite a growing body of research on the impact of urbanization on urban surface runoff, there is a notable lack in understanding urbanization-induced changes in channel runoff. As the new generation of WRF model, WRF-Hydro improves the current capability in simulating channel runoff and has been extensively explore by coupling with other sophisticated models (e.g., WRF, VIC; Quenam et al., 2022; Wang et al., 2022). Thus, it is promising to employ the WRF-Hydro to evaluate the urbanization-induced channel runoff variations within local urban extent, where data scarcity is the major issue.

The uneven distribution of urban resources in cities, resulting from unplanned and clustered development, further complicates the spatial patterns of urban runoff (Xu et al., 2020; Yao et al., 2015). Previous studies have made efforts to understand the runoff response to the urban structure caused by urbanization (Li et al., 2018; Xu et al., 2020). Nevertheless, the urban regions were generally classified into different irregular blocks based on the functions with relatively coarse resolution and limited categories, which may be not sufficient for a more thorough and accurate understanding of urbanization effects on the spatial pattern of urban runoff. Recently, the newly published local climate zone (LCZ) dataset divides the urban regions based on building height, building arrangement, and infrastructure function with high spatial resolution at pixel scale (Ching et al., 2018; Demuzere et al., 2019; Demuzere et al., 2022). The introduction of the LCZ data into the urban hydrological study has potential to offer more nuanced insights into the runoff patterns under urbanization and should be further explored (Zheng et al., 2023; Du et al., 2023).

The Yangtze River Basin (YRB) has experienced unprecedented urbanization in recent decades, encompassing over 40 cities and accommodating 33 % of China's population (Yang et al., 2021). The urbanization process has exerted substantial impact on the urban runoff responses within the YRB. Meanwhile, projections indicate a doubling of the urban area in the YRB by 2050, imposing substantial challenges on flood precaution and management (Chen et al., 2021). Thus, the major objective of this study is to establish a quantitative framework to achieve more in-depth and comprehensive understanding of urbanization effects

on the spatio-temporal characteristics of runoff. Specifically, the framework was designed to address the following key questions:

- (1) How does the urbanization process (i.e., expansion of impervious surface) affect spatial and temporal patterns of the channel and surface runoff?
- (2) What are the potential factors and mechanisms related to urbanization-induced runoff modification?

In response to these questions, the results are expected to quantitatively uncover the urbanization effects on channel and surface runoff based on both empirical and physical hydrological models within the urban extents, which would support urban environment management and policy making on runoff-related issues and disasters.

2. Study area and data

2.1. Study area

Originating from the Qinghai-Tibet Plateau, the Yangtze River is the longest river in Asia and the third longest globally. The YRB accommodates about 5.8 % of the world's population and spans an area of 1.8 million square kilometers. Recent decades have witnessed an unprecedented surge in urbanization within the YRB, boasting over 40 cities that contribute to 35.4 % of China's GDP. Meanwhile, flooding has become one of the most prevalent and destructive disasters in urban regions within the YRB. For this study, three typical urban agglomerations were selected as the study areas to investigate urbanization effects on runoff, including the Yangtze River Delta (YRD), Middle Region of Yangtze River (MYR), and Chengdu-Chongqing (CY) urban agglomerations (Fig. 1; Fang, 2015; Fang et al., 2015). The three urban agglomerations exhibit diverse terrains and hydro-meteorological characteristics. Specifically, MYR and YRD are situated in the middle and lower regions of YRB with an average elevation lower than 150 m while CY has basin terrain with an average elevation of about 584 m. In addition, the spatial distribution of precipitation varies significantly among these regions, with higher annual rainfall amount in YRD (~1300 mm) and MYR (~1500 mm) (Huang et al., 2023b). The three urban agglomerations show rapid urban expansion in recent decades due to the reform and opening-up policy and the construction of Yangtze River Economic Belt, which has posed substantial impacts on the local meteorological (e.g., precipitation, temperature, humidity) and hydrological (e.g., runoff, soil moisture) environment (Huang et al., 2023b). In such a context, a comprehensive and quantitative investigation of urbanization effects on runoff is of great significance for the flood management and adaptive decision-making.

2.2. Data

A total of three categories of datasets were adopted in this study, including remote sensing-based products, reanalysis products, and auxiliary datasets (Table 1). The detailed descriptions of the datasets are presented below.

2.2.1. Remotely sensed products

In this study, Moderate Resolution Imaging Spectroradiometer (MODIS) NDVI product—MOD13Q1 (250 m spatial resolution and 16-day temporal resolution), was adopted to analyze the land covers in the three urban agglomerations. We collected NDVI data during rainy season (May-October) in 2000, 2010, and 2020 to better capture the surface runoff characteristics in the high-flow period of study regions (Liu et al., 2021b). The quality control information was used to remove the low-quality and cloud-contaminated pixels. Finally, the NDVI data was averaged to obtain the annual mean values in each year and reprojected to UTM projection with WGS84 datum.

As a major indicator of urbanization, impervious surface area (ISA)

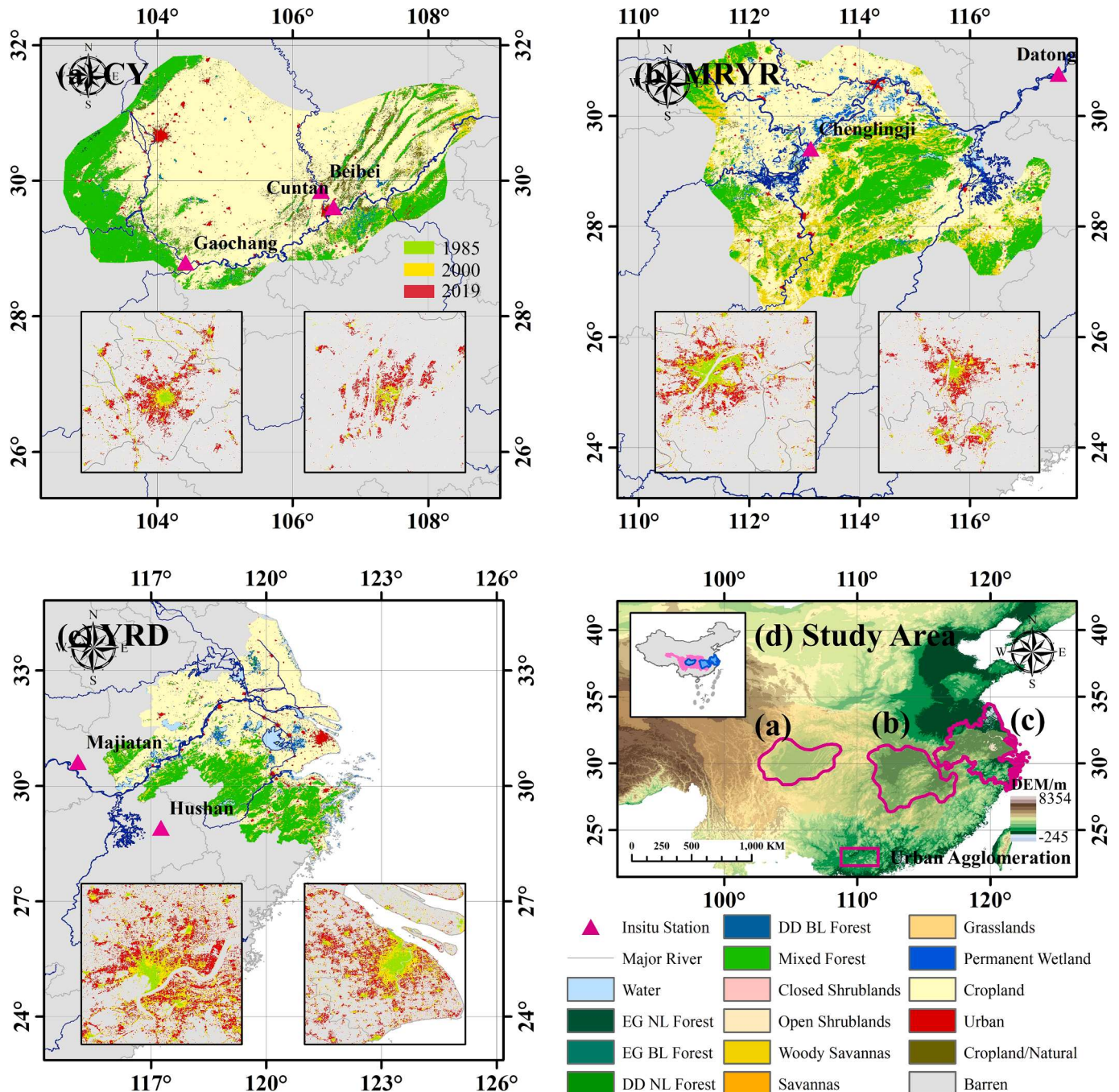


Fig. 1. The geographical location and land cover of three urban agglomerations. In the sub-figures of (a)-(c), the green, yellow, and red color represent the urban areas in 1985, 2000, and 2020, respectively. The violet triangles in (a)-(c) are the locations of in-situ hydrological stations. The blue lines are the major rivers in each urban agglomeration. (For interpretation of the references to color in this figure legend, the reader is referred to the web version of this article.)

data was considered. We acquired Global ISA (GISA2.0) dataset proposed by Huang et al., (2022b) with a spatial resolution of 30 m. Considering the inconsistency degree of current popular ISA datasets, the production of GISA2.0 divided the mapping area into A-Grids and M-Grids, coupled with automatic and manual mapping methods, respectively (Huang et al., 2022b; Hu and Huang, 2019). Currently, GISA2.0 has been widely adopted in urban-related studies and shown excellent performance compared to the existing ISA datasets.

To further investigate the detailed spatial patterns of runoff under rapid urbanization, we obtained a global map of LCZ produced by Demuzere et al. (2022). The LCZ products exhibits 100 m-resolution land cover types which are composed of 10 built types (e.g., compact/

open highrise/midrise/lowerise) and 7 natural types (e.g., dense/scattered trees, bare soil/sand, water). The quality of the global LCZ product has been validated using a bootstrap cross-validation method based on multi-source global data.

2.2.2. Model-based products

For WRF-Hydro simulation, the China Meteorological Forcing Dataset (CMFD) produced by He et al. (2020) was adopted as the meteorological forcing. CMFD has 0.1° spatial resolution and 3-hour temporal resolution. The validation against ground observations shows that CMFD outperforms other meteorological forcing datasets (e.g., GLDAS) due to the integration of a large number of in-situ

Table 1

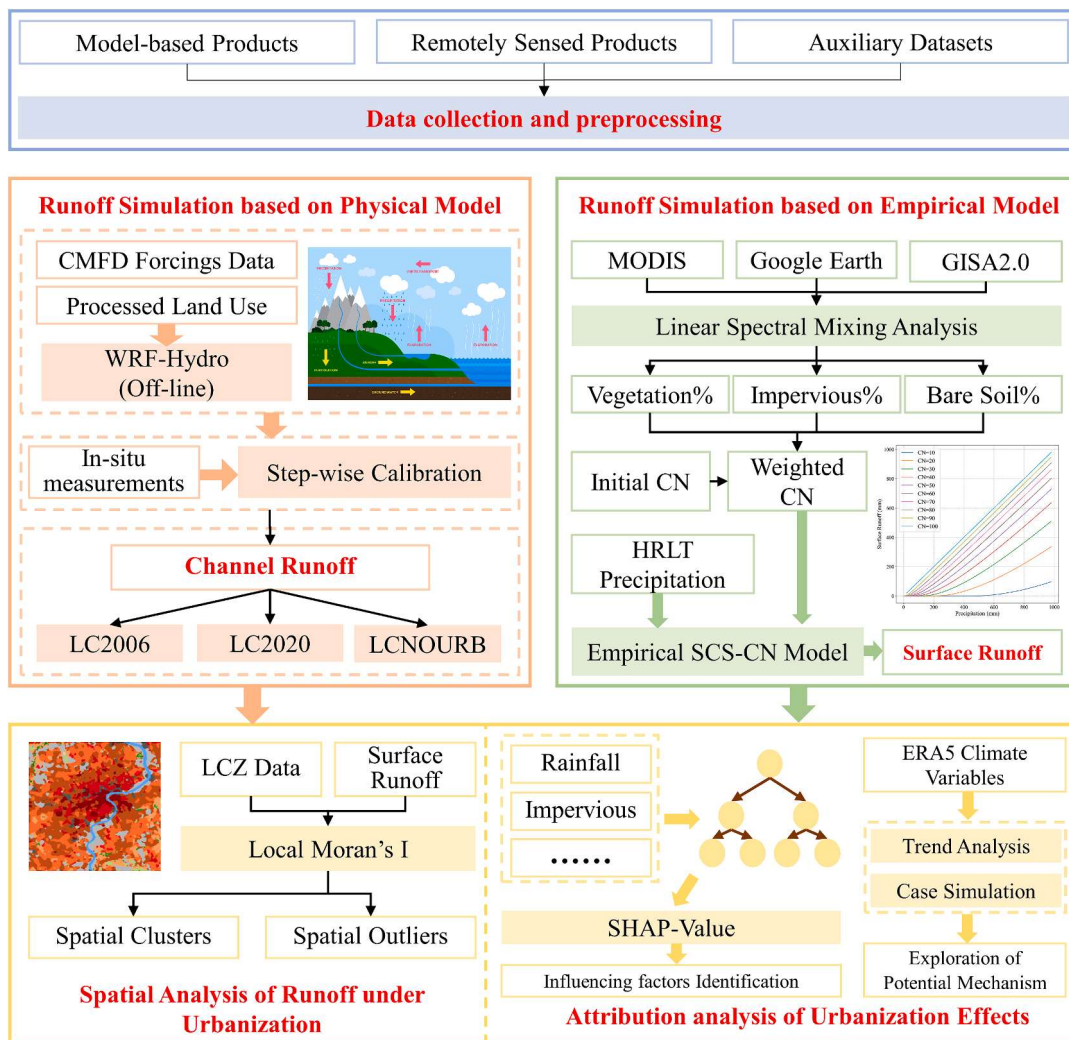
The description of the adopted datasets.

Type	Product	Variable	Spatial Resolution	Temporal Resolution	Selected Dates
Remotely sensed product	MOD13Q1	NDVI	250 m	16-day	2000, 2010, 2020
	MCD12Q1	Land cover	500 m	Yearly	2006, 2020
	GISA2.0	Impervious surface	30 m	Yearly	2000, 2010, 2020
Reanalysis product	Global LCZ	LCZ classification	100 m	/	/
	HYSOGs250m	Soil group (A/B/C/D)	250 m	/	/
	CMFD	Meteorological forcings	0.1°	3-hour	2006–2017
	HRLT	Precipitation	1 km	Daily	2006–2017
	ERA5	Precipitation, 10 m V-wind, 10 m U-wind, sensible heat flux, friction velocity, and boundary layer height	0.25°	Hourly	2008–2017
Auxiliary data	SRTM	DEM	30 m	/	/
	In-situ hydrological station	Streamflow	/	Daily	2006–2007
	Landscan	Population density	1 km	Yearly	2000, 2010, 2020
	GUB	Global urban boundary	/	5-year	2018

measurements.

For curve number (CN)-based runoff simulation, HYSOGs250m dataset developed by Ross et al. (2018) was first adopted to calculate

curve number (CN). HYSOGs250m classifies soils into four groups with different levels of runoff potential. The quality of HYSOGs250m has been validated and it has been widely used in runoff estimation and

**Fig. 2.** The methodology of the proposed quantitative analysis framework. The entire framework can be divided into four parts: (a) Data collection and pre-processing; (b) Runoff simulation based on physical model; (c) Runoff simulation based on empirical model; (d) Spatio-temporal and attribution analysis of urbanization effects on runoff.

flood assessment. Then, a High-Resolution and Long-Term (HRLT) dataset developed by Qin et al. (2022) was applied to provide precipitation and temperature data for the CN-based runoff model. The HRLT dataset has 1 km and daily resolution.

In order to further explore the potential mechanism of urbanization effects on runoff, we collected ERA5 reanalysis dataset from Climate Data Store (CDS). We selected six variables with 0.25° spatial resolution, including precipitation, 10 m V-wind, 10 m U-wind, sensible heat flux, friction velocity, and boundary layer height.

2.2.3. Auxiliary data

We collected in-situ daily channel runoff data from a total of seven hydrological stations distributed in three urban agglomerations, which were provided by Changjiang Water Resources Commission. Besides, we acquired land cover data from MCD12Q1 product, which has 500 m spatial resolution. The Shuttle Radar Topography Mission (SRTM) DEM product with a spatial resolution of 30 m was also used in this study. In order to investigate the relationship between urban runoff and population, we downloaded population distribution data from LandScan. In addition, we also adopted Global Urban Boundary (GUB) data to extract urban regions (Li et al., 2020). To ensure enough pixels in the urban boundary regions, the urban boundaries with area over 100 km² were selected (Zhang et al., 2022).

3. Methods

3.1. Methodology

The methodology of the proposed quantitative analysis framework is presented in Fig. 2. The framework contains four parts: (a) Data collection and preprocessing; (b) Runoff simulation based on physical model; (c) Runoff simulation based on empirical model; (d) Spatio-temporal and attribution analysis of urbanization effects on runoff. The detailed information of each part is elaborated in the following sections.

3.2. Channel runoff simulation based on WRF-Hydro

The distributed hydrological model, i.e., the Weather Research and Forecasting Model Hydrological modeling system (WRF-Hydro) was operated in this study to simulate channel runoff in different urbanization scenarios (Sofokleous et al., 2023). WRF-Hydro is an enhanced version of the previous WRF model coupled with the NOAH-MP land surface model (LSM), which incorporates channel, overland, groundwater flow into a modeling structure. The model has been broadly applied in the simulation and prediction of hydrological process at diverse spatial scales (from local catchment to continental river basin) and temporal resolutions (Guo et al., 2022; Zhang et al., 2021; Liu et al., 2021b).

Three nested domains were designed to cover the three urban agglomerations. WRF-Hydro can disaggregate the low-resolution LSM grids into high-resolution routing grids after the computation of moisture states for the land surface column. In this study, the LSM grid resolution was defined as 5 km and the routing grid resolution was set as 500 m. The geographical locations of three domains are shown in Fig. S1. In addition, the entire routing framework (including base flow process, channel routing, overland flow process, and subsurface flow process) was activated in three domains. The land cover was generated from the MODIS IGBP land cover category. The geographic data (i.e., DEM, flow direction, flow accumulation, and river network) was provided by Shuttle Elevation Derivatives at multiple scales (HydroSHEDS) database. Meanwhile, the WRF-Hydro runoff simulation was performed with CMFD meteorological forcings, which has relatively higher accuracy over China mainland.

During the operation of WRF-Hydro, the parameter calibration is crucial for the accurate simulation of runoff (Li et al., 2023a; Dhar et al.,

2022). In this study, the model spin-up period was set as 10 years from 1995 to 2005. Then, the model was calibrated against the observed streamflow at each domain during 2006–2007. Due to the requirement of large computation for automatic calibration, the model was calibrated manually using a step-wise method (Liu et al., 2021b; Yucel et al., 2015). Specifically, a parameter is determined at each step, and then it is passed to the calibration of the following parameters. According to the hydrological function in the WRF-Hydro model, the parameters can be classified into two groups with the ones responsible for the hydrograph volume and the shape, respectively (Xiang et al., 2017; Kilicarslan et al., 2021). In this study, a total of ten parameters were selected to calibrate WRF-Hydro simulation regarding the soil, runoff, groundwater, and channel processes (Dhar et al., 2022; Gochis et al., 2019). The detailed information about the calibrated parameters can refer to Table S1.

Based on the calibrated parameters, we designed three separate experiments with different LULC data to investigate the urbanization impacts on runoff. The control simulation (LC2006) adopted LULC data in 2006 as the reference urbanization scenario. In the second simulation, we replaced the LULC data in 2006 with LULC data in 2020, representing a highly urbanized scenario (LC2020). In the third simulation, we replaced the urban pixels in 2006 LULC with the dominant LULC type in the urban agglomeration. In other words, the LULC data in the third simulation did not contain urban pixels, and the runoff was simulated without the impact of urbanization (LCNOURB). In this study, the channel runoff from 2008 to 2017 in three scenarios were simulated. By comparing the runoff in different urbanization scenarios, the effects of urbanization on channel runoff can be quantified.

3.3. Surface runoff simulation based on SCS-CN

In addition to the WRF-Hydro based runoff modelling, we also applied the widely-adopted Soil Conservation Service-Curve Number (SCS-CN) method to simulate high-resolution surface runoff. SCS-CN is an empirical based runoff estimation method using remotely sensed data, which was developed by Soil Conservation Service and further improved by Pandit and Gopalakrishnan (1996). This method is widespread in various hydrological models (e.g., the Soil and Water Assessment Tool (SWAT), the Hydrologic Modeling System (HEC-HMS)) and the evaluation of the effects of land use changes on surface runoff from large river basin to small urban catchment. SCS-CN has limited requirements of the input parameters, which only considers initial abstraction, potential maximum retention of soil, and precipitation (Maragno et al., 2018). The simulation of runoff can be described as follows:

$$Q = \begin{cases} \frac{(P - I_a)^2}{P - I_a + S}, & P \geq I_a \\ 0, & P < I_a \end{cases} \quad (1)$$

$$S = \frac{25400}{CN} - 254 \quad (2)$$

$$I_a = \lambda \times S \quad (3)$$

where Q and P is the simulated runoff and input precipitation, respectively. λ indicates the initial abstraction coefficient, which is usually defined as 0.2. CN (ranging from 0 to 100) is the dimensionless curve number derived based on the hydrological characteristics of the land cover. A higher CN value indicates higher runoff accumulated by land surface under a given rainfall event. The tabulated CN values provided by SCS are determined by HSG, land cover, and antecedent moisture condition (AMC). In this study, AMC II was selected, which represents average/normal moisture condition.

To simulate more accurate surface runoff in the three urban agglomerations in YRB, an improved composite CN method developed by Fan et al. (2013) was utilized to calculate CN. The composite CN for each

pixel can be calculated based on a weighted formula as follows:

$$CN_C = P_I \times CN_I + P_V \times CN_V + P_S \times CN_S \quad (4)$$

where CN_I , CN_V , and CN_S are the initial CN values for impervious area, vegetated area, and bare soil, respectively. P_I , P_V , and P_S are the percentages of impervious, vegetation, and bare soil areas in each pixel, respectively. The initial CN values of bare soil and vegetation under AMC II level are shown in Table S2-S3. The percentages of impervious, vegetation, and bare soil in each pixel were retrieved by a linear spectral mixing analysis (LSMA) approach (Zhang et al., 2018b). LSMA follows a vegetation-impervious surface-soil (V-I-S) concept, which can be described as follows:

$$P_I + P_V + P_S = 1, \quad 0 \leq P_I \leq 1, \quad 0 \leq P_V \leq 1, \quad 0 \leq P_S \leq 1 \quad (5)$$

The 250 m MOD13Q1 NDVI images were input into LSMA and an inverse least squares deconvolution approach was used to retrieve the proportions of V-I-S (Liu et al., 2021b). The detailed calculation of composite CN values can then refer to Supporting Information (SI) Text S1. In order to simulate the surface runoff in different urbanization scenarios, we calculated the composite CN based on the NDVI and land cover in 2000, 2010, and 2020. And the 250 m SCS-CN based surface runoff in three urbanization scenarios (i.e., LC2000, LC2010, LC2020) was finally computed by inputting HRLT precipitation and composite CN in three urban agglomerations.

3.4. Spatio-temporal and attribution analysis methods

3.4.1. Trend analysis

Trend analysis was conducted to study the temporal patterns of runoff and runoff-related patterns under different urbanization scenarios. Specifically, Mann-Kendall (MK) trend test and Sen's slope were adopted to evaluate the trend of the time series. Sen's slope is a non-parametric trend estimation approach developed by Sen (1968), which can be described as follows:

$$\beta = \text{median}\left(\frac{x_j - x_i}{j - i}, \forall j > i\right) \quad (6)$$

where x_i and x_j are a certain time series at time i and j . The positive/negative value of Sen's slope indicates that the time series has an increasing/decreasing trend. Further, MK trend test was used to evaluate the significance of the trend slope (Mann, 1945; Kendall, 1948). The MK-Z value can be obtained as:

$$Z = \begin{cases} \frac{S}{\sqrt{\text{Var}}} & (S > 0) \\ 0 & (S = 0) \\ \frac{S + 1}{\sqrt{\text{Var}}} & (S < 0) \end{cases} \quad (7)$$

where $S = \sum_{i=1}^{n-1} \sum_{j=i+1}^n \text{sign}(x_j - x_i)$ and $\text{Var} = n(n-1)(2n+5)/18$. n is the number of samples. In this study, the null hypothesis (without significant trend) was rejected at 5 % significance level when $|Z| > 1.96$.

In order to quantify the urbanization effects on runoff, the trend values of urban and rural runoff series were calculated based on Sen's slope and MK methods, which were denoted as T_u and T_r , respectively. Further, the urbanization effect and contribution were quantified as $T_u - T_r$ and $|(T_u - T_r)/T_u| \times 100\%$, which have been widely adopted in previous urbanization-related studies (Huang et al., 2023b; Yu et al., 2022).

3.4.2. Moran's I

In order to explore the spatial pattern of runoff under urbanization, local Moran's I was used to calculate the spatial autocorrelation as a local indicator of spatial association (LISA). The local Moran's I index was calculated for each pixel in the study area to classify them into

spatial clusters and outliers (Yuan et al., 2018). Local Moran's I index can be expressed as:

$$I_i = \frac{z_i - \bar{z}}{\sigma^2} \sum_{j=1, j \neq i}^n [W_{ij}(z_j - \bar{z})] \quad (8)$$

where I_i is the local Moran's I index. z_i is the runoff at location i . \bar{z} represents the mean runoff value. z_j denotes the runoff value at other location. σ^2 is the variance of z . W_{ij} indicates the spatial weight of z_i and z_j . The positive local Moran's I value demonstrates that the location has similarly high or low value as its surrounding pixels (i.e., spatial cluster) while the negative value indicates a potential spatial outlier. The resulted clusters are recognized based on four types of spatial associations: high values surrounded by high values (HH), low values surrounded by low values (LL), high values surrounded by low values (HL), and low values surrounded by high values (LH).

3.4.3. LightGBM and SHAP-value

In order to further analyze the underlying mechanism of the urbanization effects on runoff, we adopted LightGBM and Shapley Additive exPlanations (SHAP) value to explore the potential factors affecting urban runoff. LightGBM is one of the most powerful and state-of-the-art machine learning models, which is developed by Microsoft Research based on boosting regression and histogram-based algorithms (Ke et al., 2017; Bai et al., 2022; Bai et al., 2023). The utilization of histogram-based approaches increases the speed of training and reduces the memory usage. In addition, the implementation of leaf-wise tree grow algorithm in LightGBM makes it achieve a lower loss. In this study, the SCS-CN based surface runoff was chosen as the response variable. Six variables were selected as the predictors, including precipitation, NDVI, DEM, impervious surface percentage (ISP), LCZ, and population.

With the optimized LightGBM models, the SHAP technique was performed to obtain the relative importance and influence of these factors on urban runoff. The SHAP framework is proposed by Lundberg and Lee (2017) based on the calculation of Shapely value to determine how the input features affect the response variable of the given model. In these years, SHAP-value has been widely adopted in the interpretation of machine learning models (especially tree models), which facilitates more in-depth understanding of the black-box of the machine learning models.

4. Results

4.1. Evaluation of surface and channel runoff

Before the investigation of urbanization effects on channel and surface runoff, we evaluated the model performance of the WRF-Hydro simulation. In this study, ten parameters related to the hydrograph volume and shape were calibrated to enhance the accuracy of runoff simulation. The simulated channel runoff was assessed against the observed streamflow from the hydrological stations distributed in three domains during 2006–2007. Three metrics (Pearson correlation coefficient (PCC), Root Mean Squared Error (RMSE), and Nash-Sutcliffe efficiency coefficient (N-SC)) were selected to evaluate the performance (Li et al., 2022). The validation results at each hydrological station are shown in Fig. 3. Generally, the simulated runoff showed good agreement with the observed streamflow. The average PCC and N-SC over three urban agglomerations achieved 0.856 and 0.624, respectively. The peaks of the simulated channel runoff matched well with the observed streamflow. Although the PCC at Datong station in MRYR achieved 0.821, the N-SC exhibited relatively poor performance, which were 0.289. This discrepancy can be attributed to Datong station's location on the Yangtze River's trunk stream, resulting in a larger runoff volume compared to tributary stations. The MRYR domain, covering only a portion of the trunk stream and not considering the upstream section, led to the underestimation of channel runoff at Datong station. Overall,

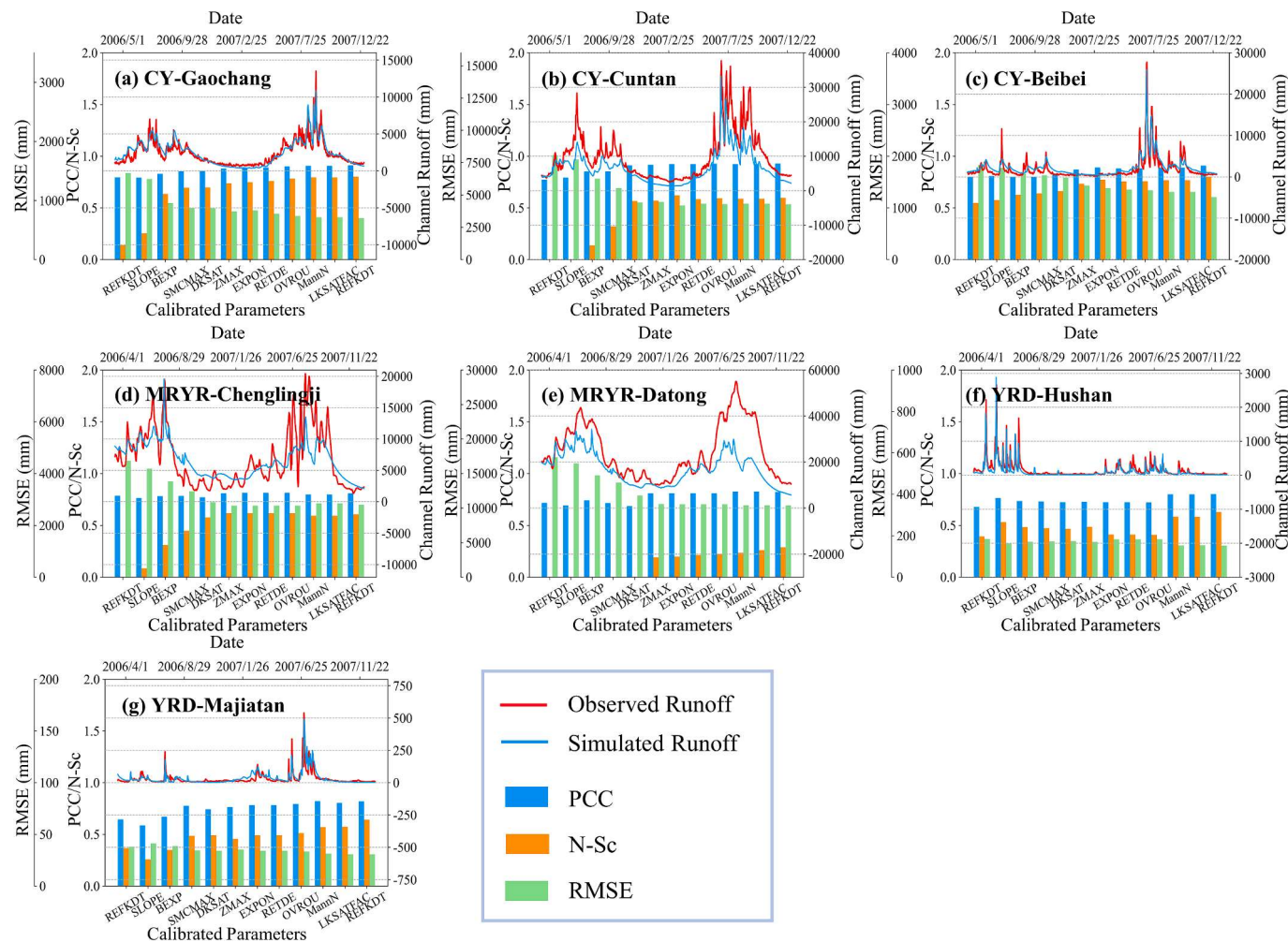


Fig. 3. The validation of the simulated channel runoff based on WRF-Hydro against observed streamflow. The red and blue lines represent observed streamflow and simulated channel runoff, respectively. The blue, orange, and green bars indicate PCC, N-Sc, and RMSE, respectively. The labels of the bottom x-axis from left to right are the orders of calibrated parameters. (For interpretation of the references to color in this figure legend, the reader is referred to the web version of this article.)

the evaluation of the channel runoff confirmed that the outputs of the calibrated WRF-Hydro model were able to support the subsequent analysis.

For the validation of the SCS-CN surface runoff, we visualized the composite CN values integrated with the percentages of ISA, vegetation, and bare soil areas in different urbanization scenarios (Fig. S2). It can be seen that the average CN values in the major urban regions (circled areas) at three urban agglomerations showed a significantly increasing trend with the urban expansion. Results demonstrated that the core urban areas would have more accumulated surface runoff under rainfall events. Further, the HRLT precipitation data was used to produce surface runoff data based on SCS-CN model. Due to the lack of in-situ surface runoff measurements in the cities, we evaluated the performance of SCS-CN surface runoff by comparing with ERA5-Land runoff data. The comparison results are presented in Fig. S3. In general, the SCS-CN surface runoff showed high correlation with ERA5-Land runoff in three urban agglomerations. Nevertheless, results showed that the SCS-CN surface runoff was overestimated during the comparison. It can be attributed to various factors such as the differences of the spatial resolution (250 m SCS-CN surface runoff and 0.1° ERA5-Land surface runoff) and the input precipitation datasets. Previous studies also encountered similar issues when comparing the model-based runoff with other runoff datasets (Wang et al., 2015; Liu et al., 2021b; Du et al., 2012). Significantly, as noted by Wang et al. (2015), since all simulations here were conducted by the same models (WRF-Hydro or SCS-CN)

and showed similar temporal characteristics, the discrepancies could be considered as the systematic model error, which would not affect the internal model comparisons.

4.2. Urbanization effects on surface and channel runoff

To quantify the urbanization effects on the runoff variations, we initially calculated the variation rates of channel runoff between different urbanization scenarios in three urban agglomerations. Fig. 4 illustrates results for the largest city in each agglomeration (Chengdu in CY, Wuhan in MRYR, Shanghai in YRD). Here, LC2006, LC2020, and LCNOURB represent the runoff simulation in the control scenario, highly urbanized scenario, and non-urbanization scenario, respectively. The variations in channel runoff were assessed along the urban–rural gradient, with outward buffers from each urban region serving as rural areas (detailed procedure refers to SI Text S2). Common features across different scenarios showed an overall increase in channel runoff from low to high urbanization cases, with more pronounced increases in urban regions than surrounding rural areas (Debbage and Shepherd, 2018). Fig. S4 depicts the distributions of the change rates in urban and rural regions for different scenarios. The change rates in urban areas exhibited prominent positive values, signifying an increase in channel runoff due to urbanization. Urban areas are densely distributed with impervious surfaces, hindering the infiltration of runoff and causing it to flow directly into rivers, ultimately increasing channel runoff (Zhang

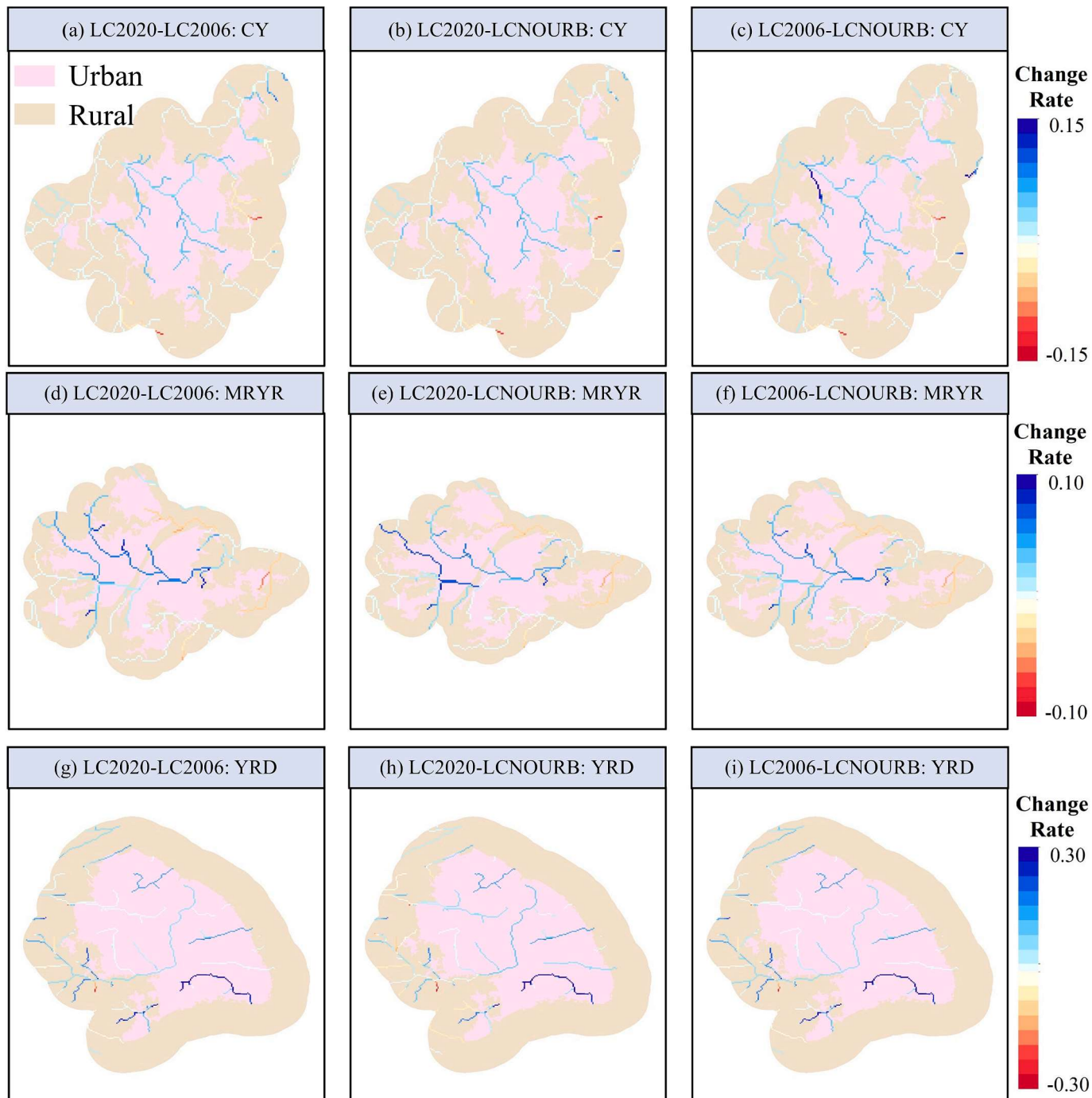


Fig. 4. The change rates of channel runoff in the comparison of different scenarios. Specifically, the first column to the third column represent the change rates from LC2020 to LC2006, LC2020 to LCNOURB, and LC2006 to LCNOURB, respectively. One typical city in each urban agglomeration (i.e., Chengdu in CY urban agglomeration, Wuhan in MRYR urban agglomeration, and Shanghai in YRD urban agglomeration) is selected for the visualization. The pink and brown regions indicate the urban and rural regions for each city. The determination of the rural region can refer to SI Text S2. (For interpretation of the references to color in this figure legend, the reader is referred to the web version of this article.)

et al., 2018b; Schoener, 2018; Li et al., 2019). Among three scenarios, LC2020-LCNOURB represented more significant increasing rates due to the more significant urbanization differences between LC2020 and LCNOURB. On average, the urbanization led to the increase of channel runoff in three urban agglomerations by 4.4 %, 5 %, and 12.08 %, respectively.

Fig. 5 exhibits the seasonal variations of channel runoff and the corresponding urbanization effects in different scenarios in three urban agglomerations. Seasonal channel runoff, which were further

categorized into quartiles, exhibited significant seasonality, with higher total volume and peak (75-100th) volume in summer and autumn than that in spring and winter. The urbanization effects also demonstrated a similar seasonality, exerting more influence on channel runoff in summer than other seasons, with the lowest impact in spring. We attribute the seasonality to the rainfall variations in the YRB, aligning with the high-flow and low-flow seasons in major rivers during summer and winter. High-flow seasons witness increased channel runoff due to concentrated rainfall under the summer monsoon circulation and spring

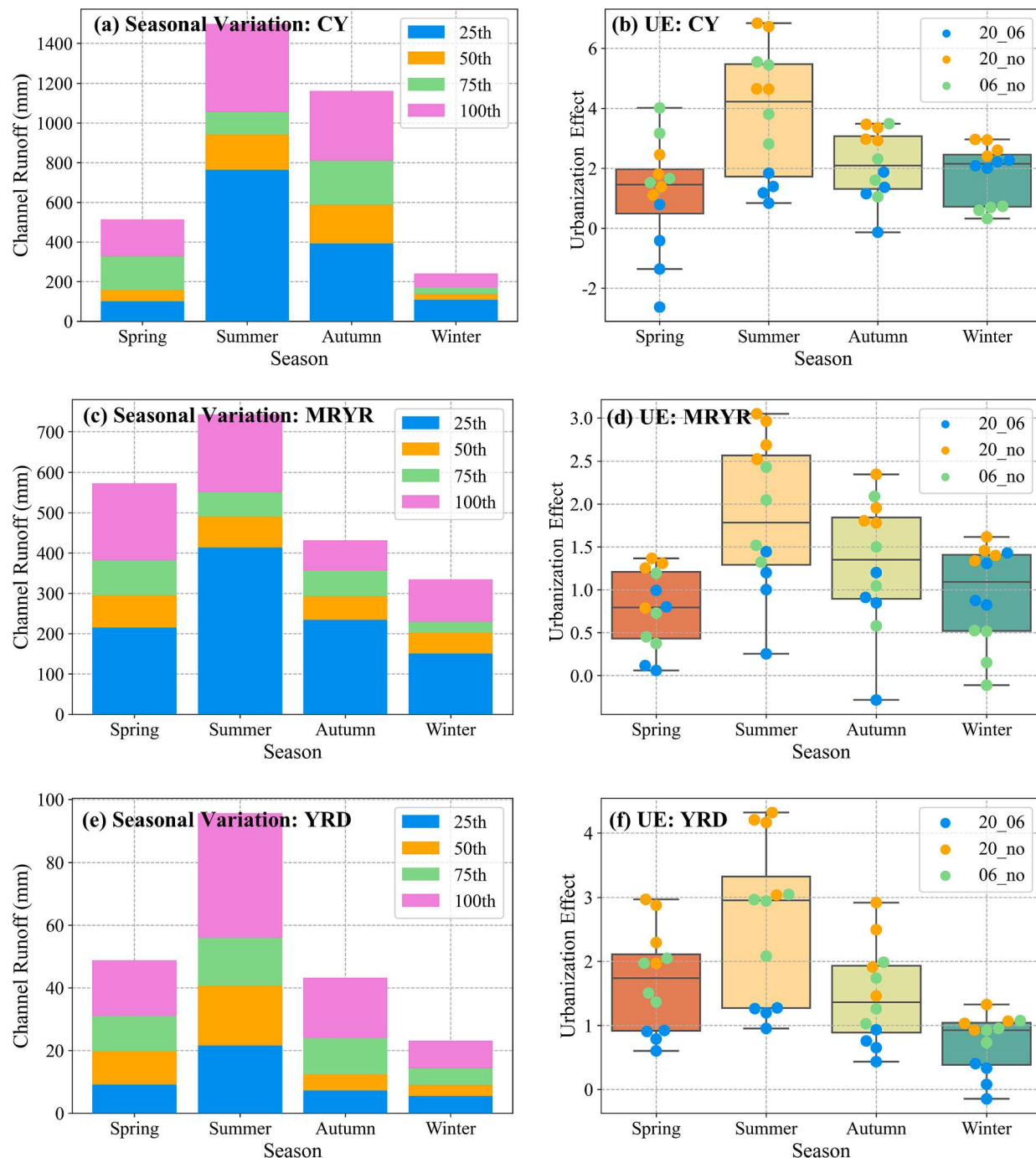


Fig. 5. The seasonal variations of channel runoff in different percentiles and urbanization effects (UE) in different scenarios. The blue, orange, green, and violet bars in the first column are the classified channel runoff at 0-25th, 25-50th, 50-75th, 75-100th, respectively. The scatter points in the second column represent the urbanization effects on the classified in different scenarios. (For interpretation of the references to color in this figure legend, the reader is referred to the web version of this article.)

atmospheric thermodynamic states exceeding the infiltration capacity of urban impervious surface.

Liu et al. (2021b) decomposed the effects of human and climate on the runoff and found that precipitation and urbanization showed the most important roles in enhancing runoff in the high-flows seasons, which corroborated with the finding in this study. Nevertheless, the response of channel runoff on the urbanization can be affected by many factors, which limits the comprehensive quantification and thus requires further in-depth study.

Fig. S5 shows the monthly surface runoff variations in urban and rural areas for different urbanization scenarios. The surface runoff also

represented obvious seasonality from 2008 to 2017. Notably, urban regions exhibit higher surface runoff, particularly during heavy rainfall events. With rising urbanization levels, surface runoff differences between urban and rural regions increase, indicating intensified urbanization effects. To quantify the urbanization effects on surface runoff, we calculated the deseasonalized surface runoff based on moving average method and applied trend analysis (Fig. 6). The deseasonalized surface runoff in urban and rural areas indicated an increasing trend from 2008 to 2017. Urban regions showed a more prominent trend than rural areas, underscoring the positive effects of urbanization on surface runoff. We further calculated the urbanization contribution on the changes of

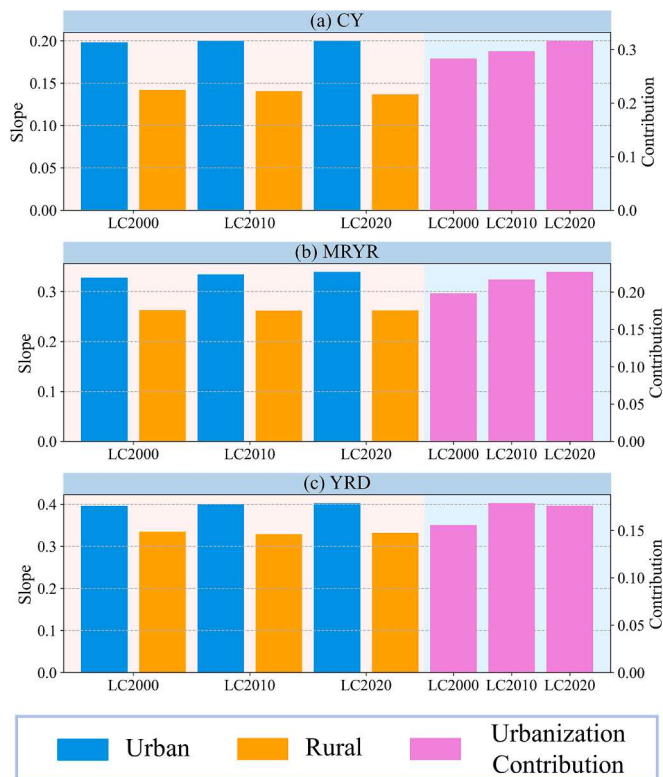


Fig. 6. The urbanization effects and contribution on surface runoff in different urbanization scenarios in three urban agglomerations. The blue and orange bars indicate the trend slope of surface runoff in urban and rural regions, respectively. The violet bar means the urbanization contribution. (For interpretation of the references to color in this figure legend, the reader is referred to the web version of this article.)

surface runoff. Results illustrated that urbanization accounted for 30 %, 21.4, and 17.7 % of the surface runoff changes in CY, MRYR, and YRD, respectively.

4.3. Case simulation in different urbanization and rainfall scenarios

The modifications of underlying surface characteristics and natural drainage network during rapid urbanization have been confirmed to increase the risk of flood hazard (Schmitt et al., 2004). To further investigate the urbanization effects on channel runoff, we simulated channel runoff during specific flood events under various urbanization scenarios. During the summer of 2010, under the influence of continuous heavy rainfall, the middle and lower regions of YRB experienced the unprecedented flood events with the highest water level in the preceding two decades. Consequently, we selected the three largest urban regions in each urban agglomeration to observe the channel runoff patterns under different urbanization scenarios (Fig. 7). Heavy rainfall occurred in each city during the designated month in 2010, with the channel runoff in three urbanization scenarios displaying notable peak values after these intense rainfall events. To provide a clearer illustration of the urbanization effects on channel runoff during flood events, we calculated channel runoff differences between the three urbanization scenarios during the peak events, as shown in the sub-figures. In general, results demonstrated that urbanization exerted more profound positive effects on the increase in channel runoff during the peak period, leading to higher risk of damage from flood hazards. Among the comparison of urbanization effects, LC2020-LCNOURB showed a more substantial increase in channel runoff, highlighting the positive relationship between the urbanization process and flood risk.

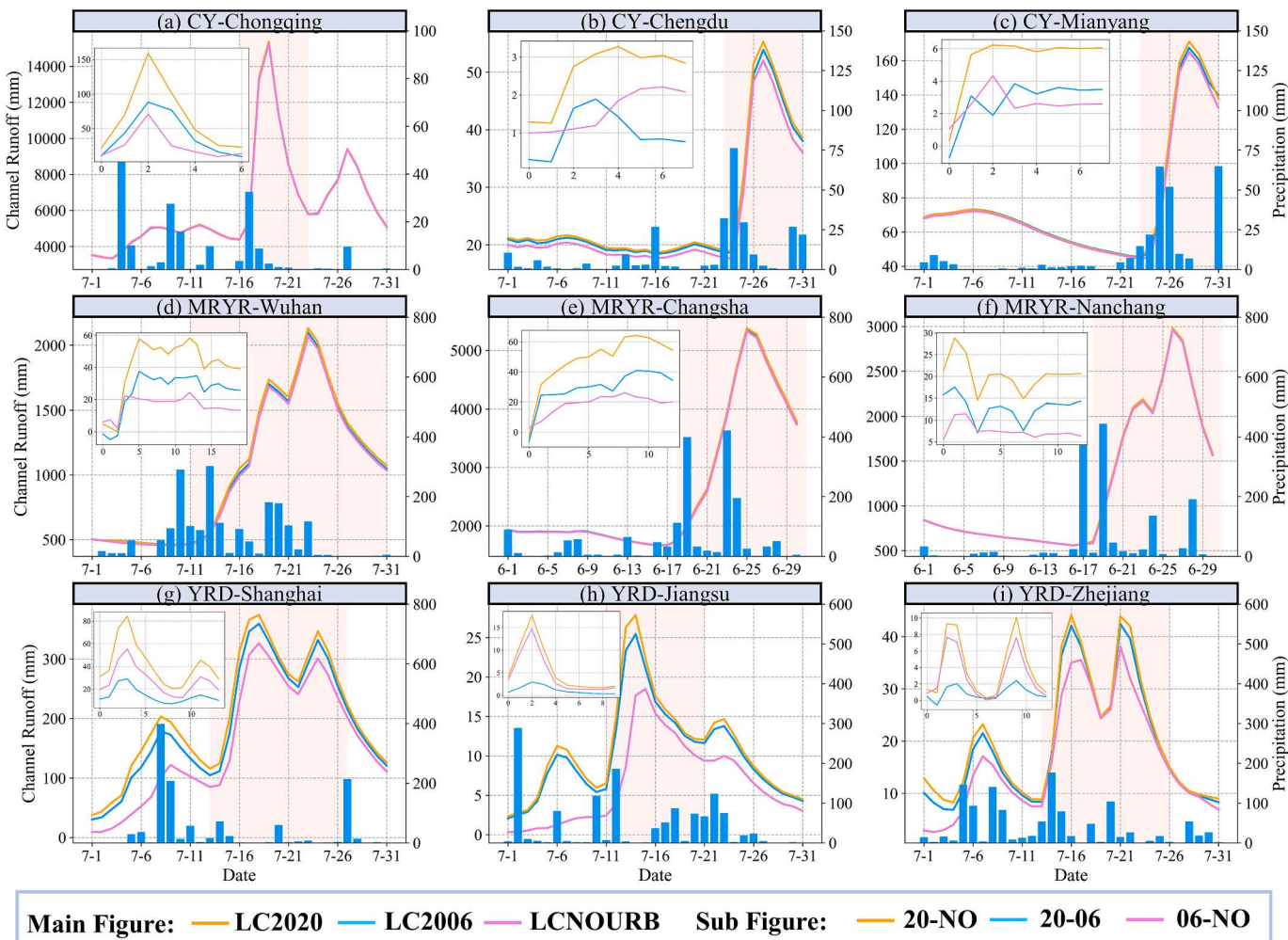
We also simulated the surface runoff under the extreme (99th of the

climatological rainfall) rainfall situation in different urbanization scenarios. The spatial distributions of surface runoff under heavy rainfall in the typical city of three urban agglomerations are presented in Fig. 8. In the case of LC2000, the high surface runoff generally concentrated in the core urban regions of each city due to the low infiltration capability caused by impervious surface. With the replacement of land surface under rapid urbanization process, the cities suffered increased pressure from the accumulated surface runoff under heavy rainfall. For instance, in the case of LC2020, the regions with high surface runoff expanded to almost the entire urban regions. By calculating the change rates of surface runoff between the cases of 2020 and 2000, results showed that the developed areas (e.g., the outer ring of the city) during the two decades experienced a more prominent increase in surface runoff, while the increase in surface runoff in the urbanized regions (e.g., core urban region) was not as significant. It was mainly due to the urbanization process progressing from the central areas of the cities in 2000 to the outer rings in 2020, as illustrated in Fig. S6. The fourth column of Fig. 8 exhibits the statistical distribution of change rates in three cities. Results demonstrated that three cities experienced prominent increase in surface runoff, with major change rates between 0 and 20 %, which was identical with the analysis above. The violet regression lines also show the significant positive relationship between the change rate and impervious surface increment between the two cases, indicating that urbanization increased surface runoff.

4.4. Spatial patterns of urbanization effects on runoff

In addition to the direct impacts on the surface and channel runoff, urbanization also exerted substantial effects on the spatial pattern of urban runoff. Urban resources (e.g., buildings, green space, impervious areas) are usually disproportionately distributed in the urban regions due to the unplanned and clustered urban expansion. To explore the spatial pattern of surface runoff under urbanization, we adopted high-resolution LCZ data and made attempt to understand the relationship between urban surface runoff and LCZ. Here the LCZ was classified into five groups, including high-rise (HR), mid-rise (MR), low-rise (LR), other buildings (OB; e.g., industry, business areas), and vegetated (VG) regions. The building areas were further classified into compact areas (CP) and open areas (OP).

Firstly, we calculated the annual surface runoff for each LCZ type in three urban agglomerations, as shown in Fig. 9. Clear differences can be observed in the distributions of annual runoff in the urban regions. Specifically, HR regions showed the largest annual surface runoff, followed by MR and LR areas. The annual runoff in CP regions was also significantly higher than in OP regions. The differences were primarily attributed to the varied functions of these urban areas. In general, HR/MR and CP regions constituted the major residential zones, concentrating dense buildings and population, mostly covered by impervious surfaces (e.g., roads). In contrast, LR areas were usually distributed in the newly developed or sub-urban regions with a lower proportion of impervious surface and population. The soil infiltration capacity was weakened with the increase of impermeable surface in the HR/MR and CP regions, which further led to the accumulation of more annual surface runoff. The VG areas generally had the lowest annual surface runoff due to the water demands of vegetation and strengthened soil infiltration. In addition, Yoo et al. (2021) modelled the rainfall-runoff process under high-rise buildings and also found that the building height and building wall had significant influences on the increase of surface runoff and peak flow through intercepting rainwater and affecting wind pattern. We also calculated the peak runoff ratio for each LCZ type in three urban agglomerations. Apart from CY, high-density regions exhibited significantly higher peak ratio than low-density regions. The peak ratio of CP regions in MRYR and YRD achieved 30.8 % and 33.4 %, respectively. The results demonstrated that, compared with low-density and vegetated areas, the dense-distributed regions suffered a higher risk of flood hazard under urbanization.



Main Figure: — LC2020 — LC2006 — LCNOURB **Sub Figure:** — 20-NO — 20-06 — 06-NO

Fig. 7. Channel runoff simulation in the cities of three urban agglomerations under the flood events in 2010. The orange, blue and violet lines in (a)-(i) represent channel runoff in the scenarios of LC2020, LC2006, and LCNOURB, respectively. The blue bar chart indicates the rainfall amount. The orange, blue and violet lines in the sub-figures represent the channel runoff differences in the scenarios of LC2020-LCNOURB, LC2020-LC2006, and LC2006-LCNOURB, respectively. (For interpretation of the references to color in this figure legend, the reader is referred to the web version of this article.)

We also adopted local Moran's I index to identify the spatial clusters and outliers of urban surface runoff. In Fig. 10, the pink, red, light-blue, and deep-blue represent HH (high values surrounded by high values), HL (high values surrounded by low values), LL (low values surrounded by low values), and LH (low values surrounded by high values) groups, respectively. The HH clusters were typically concentrated in the core urban regions and along riversides, indicating a higher risk of flood hazard under heavy rainfall events. Conversely, the LL clusters were mainly concentrated in the outer-ring of the cities, representing lower runoff-related hazard risk. The LH and HL outliers sparsely distributed in the urban areas. Specifically, the LH outliers were generally distributed surrounding the HH clusters, presenting opportunities to establish drainage networks or channels to alleviate runoff pressure at HH clusters. Furthermore, we investigated the Moran's I Index at each LCZ type in three urban agglomerations. Prominent discrepancies of HH and LL proportions can be observed in different LCZ types. HH clusters were more concentrated in HR, MR, OB, and CP regions, indicating higher runoff accumulation ability. In comparison, LR and VG regions had higher LL cluster percentage due to the greater ability of urban green spaces to store precipitation and mitigate flood hazards. Overall, under the rapid urban expansion, the spatial pattern of urban surface runoff also experienced substantial modification. Therefore, a comprehensive analysis of the spatial distribution of urban runoff and its relationship with urban functional zones would give supports and facilitate urban

flood policy making.

5. Discussion

5.1. Potential mechanism of urbanization effects on runoff

To elucidate the potential mechanisms underlying the urbanization effects on runoff, we depicted the temporal variations of several runoff-related factors (e.g., boundary layer height, friction velocity, sensible heat flux, air temperature) and mapped their spatial distributions under a given storm rainfall event. Fig. 11a-d presents the variations of runoff-related factors for the urban and rural regions. In general, urban regions exhibited a more pronounced increasing trend in friction velocity, sensible heat flux, and air temperature compared to rural regions. While the boundary layer height was higher in urban areas, the variation did not show a significant trend. To gain a deeper understanding of the interaction and impact of these variables on runoff, we mapped their distributions in the YRD on August 8, 2012, when the typhoon Haikui landed. The wind divergence/convergence, calculated based on the U-wind and V-wind components, was used to visualize how the urban environment enhanced near-surface convergence (Fig. 11e). The enhancement of convergence was observed in the urban areas of YRD, creating favorable conditions for the rainfall. Previous studies have confirmed that urban land use modifications could enhance the convergence along

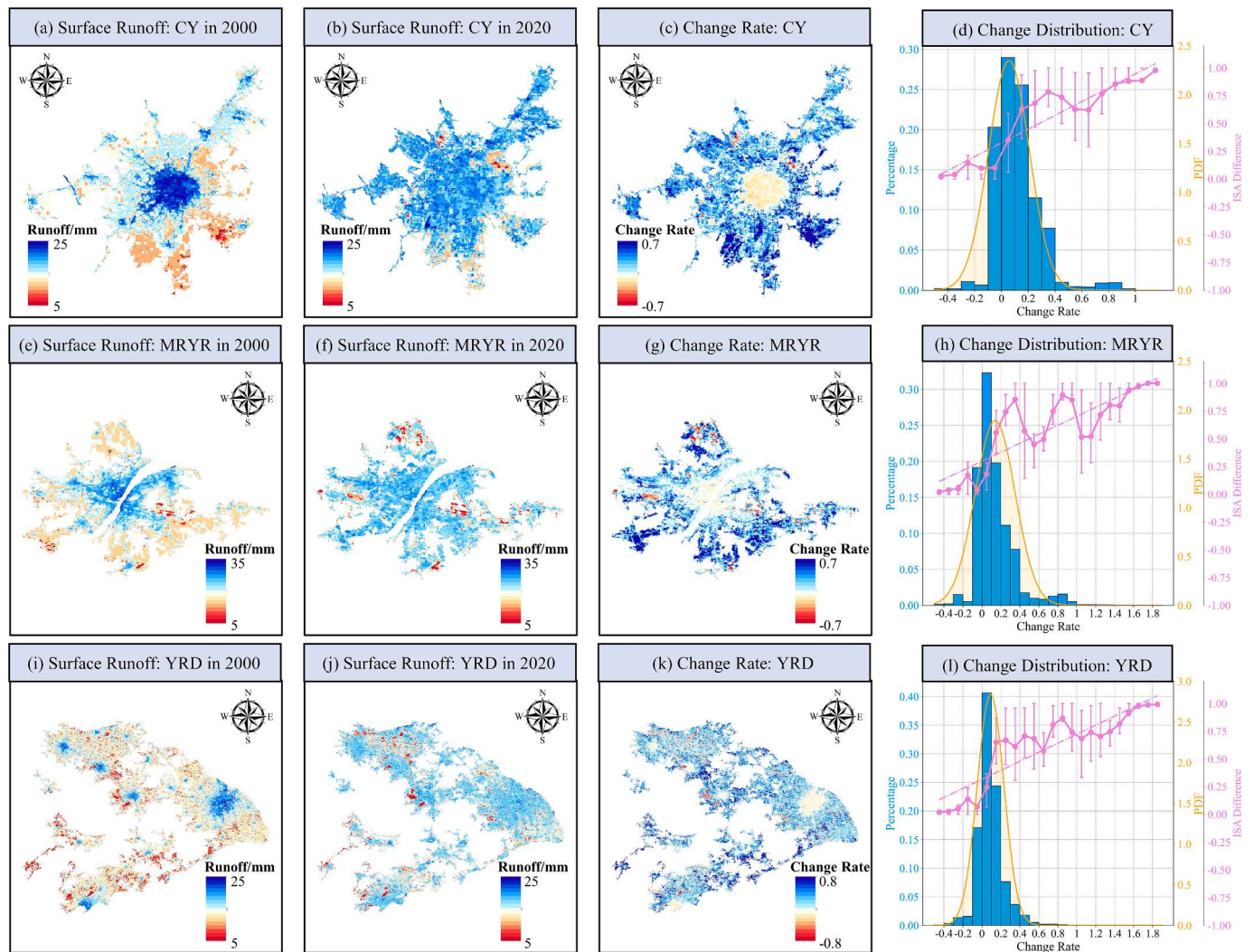


Fig. 8. Simulation of surface runoff under extreme (99th) rainfall in the typical cities in three urban agglomerations. The first and the second columns show the spatial distribution of surface runoff under heavy rainfall in the case of LC2000 and LC2020. The third column shows the change rate of surface runoff between LC2020 and LC2000. The blue bar charts in the fourth column exhibit the statistical distributions of change rate. The violet regression line represents the relationship between change rate (x-axis) and impervious surface increment (y-axis). (For interpretation of the references to color in this figure legend, the reader is referred to the web version of this article.)

urban–rural interface (Shem and Shepherd, 2009). The difference of convergence and air temperature between urban and rural areas also highlighted the existence of cyclonic flow in the moisture flux, particularly near the urban regions of YRD (Fig. 11j), which further facilitated the precipitation (Zhang et al., 2018b). These differences in convergence may be attributed to the drag of urban surface with larger roughness due to the expansion of impervious areas. Li et al., (2023b) also demonstrated the positive relationship between runoff and the climatic factors such as wind speed and relative humidity. Fig. 11c indicates that the friction velocity is prominently higher in the urban regions than in surrounding areas. Results illustrated the presence of stronger drag on the storm winds in urban regions, which further contributed to the enhancement of convergence and bifurcation of surface flow (Thielen et al., 2000). In addition, the differences of sensible heat flux between urban and rural areas associated with urbanization may also exert negative effects on the stability of the atmosphere and trigger convective precipitation. Meanwhile, the UHI effects induced by warming in urban areas and increased surface roughness also elevated the atmospheric boundary layer and further intensified precipitation.

In addition to the enhancement of precipitation, urbanization also exerted substantial effects on runoff by modifying urban land use and

underlying surface. The urbanization usually led to the destruction of original natural underlying surface (e.g., bare soil, water, grassland), replacing with urban underlying surface (e.g., roads, buildings) which had significant increase in the impermeability rate. Our statistical based attribution analysis also highlighted the importance of NDVI and LCZ types in regulating the urban runoff, as can be seen in SI Text S3 and Fig. S7. Such modifications affected the urban hydrological process, including the reduction in interception and infiltration, and increase in net precipitation. The combined effects of the urbanization on local climate and underlying surface resulted in the strengthened channel and surface runoff during the same rainfall event.

5.2. Limitations and implications

Like previous researches, this study was also subject to some limitations. Firstly, the quantitative results of this study were sensitive to WRF-Hydro model. For each urban agglomeration, 2–3 hydrological stations were collected to calibrate the WRF-Hydro model. Future modelling can acquire more in-situ stations towards better simulation accuracy. In addition, for the urban hydrological studies, the high-resolution LCZ dataset can be considered in the WRF-Hydro

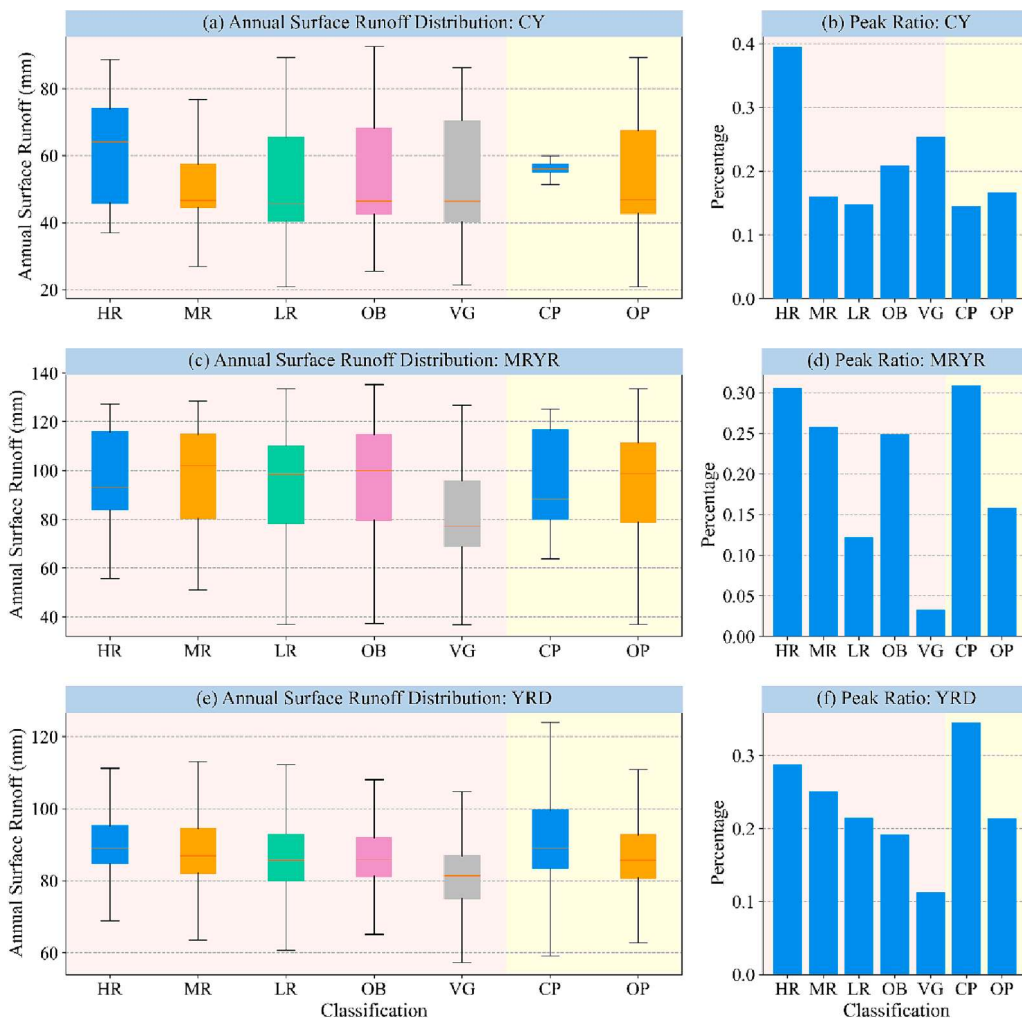


Fig. 9. The annual surface runoff and peak ratio distributions in different LCZ categories in three urban agglomerations. HR, MR, LR, OB, VG, CP, and OP represent high-rise buildings, middle-rise buildings, low-rise buildings, other buildings, vegetated regions, compact regions, and open regions, respectively. Here the monthly surface runoff over 80% of the long-term surface runoff is regarded as peak runoff.

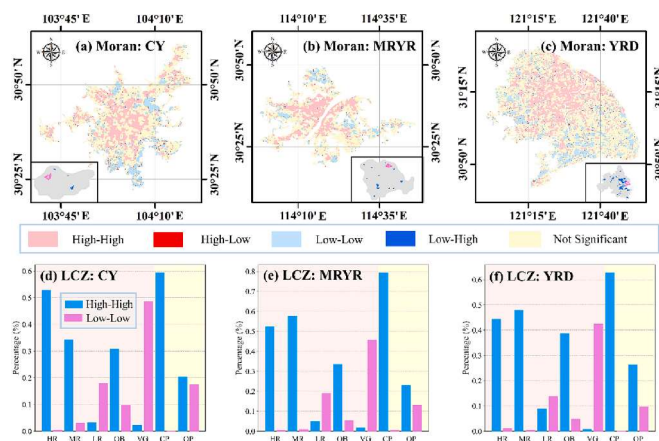


Fig. 10. The spatial patterns of surface runoff in three urban agglomerations based on local Moran's I method. The local Moran's I method divides the pixels into four types, including high-high (HH) cluster, high-low (HL) cluster, low-low (LL) cluster, and low-high (LH) cluster. The second row shows the HH (blue) and LL (violet) distributions in different LCZ categories. (For interpretation of the references to color in this figure legend, the reader is referred to the web version of this article.)

simulation, which may enable more in-depth understanding of the physical mechanism responsible for urban effects on the runoff. Secondly, the application of SCS-CN in the surface runoff simulation also existed uncertainties. The SCS-CN simplifies the consideration of various meteorological, hydrological, and land surface factors, which only requires the inputs of precipitation and pre-defined CN values based on land use and soil groups. Besides, the SCS-CN fails to consider the urban stormwater management and physical characteristics (e.g., drainage system) (Maragno et al., 2018). The intrinsic simplification of the physical process and runoff-related factors makes the SCS-CN method difficult to simulate surface runoff precisely. Nevertheless, the simplicity of SCS-CN model also makes it an effective tool for the surface runoff simulation at ungauged catchments or urban regions where the parameters required by more complicated physical models are not available (Satish Kumar et al., 2013). Considering the major objective of this study was to evaluate the relative changes of surface runoff in different urbanization scenarios (rather than the precise estimation of runoff) and all the inter-comparison simulations were conducted by SCS-CN model, the discrepancies against observations could be regarded as systematic model error, which had limited effects on the results (Maragno et al., 2018; Wang et al., 2015).

From the perspective of urban planning, the results in this study could also give implications about the mitigation of runoff increment under rapid urbanization. On one hand, it is widely acknowledged that the increase of impervious surface induced by urbanization leads to

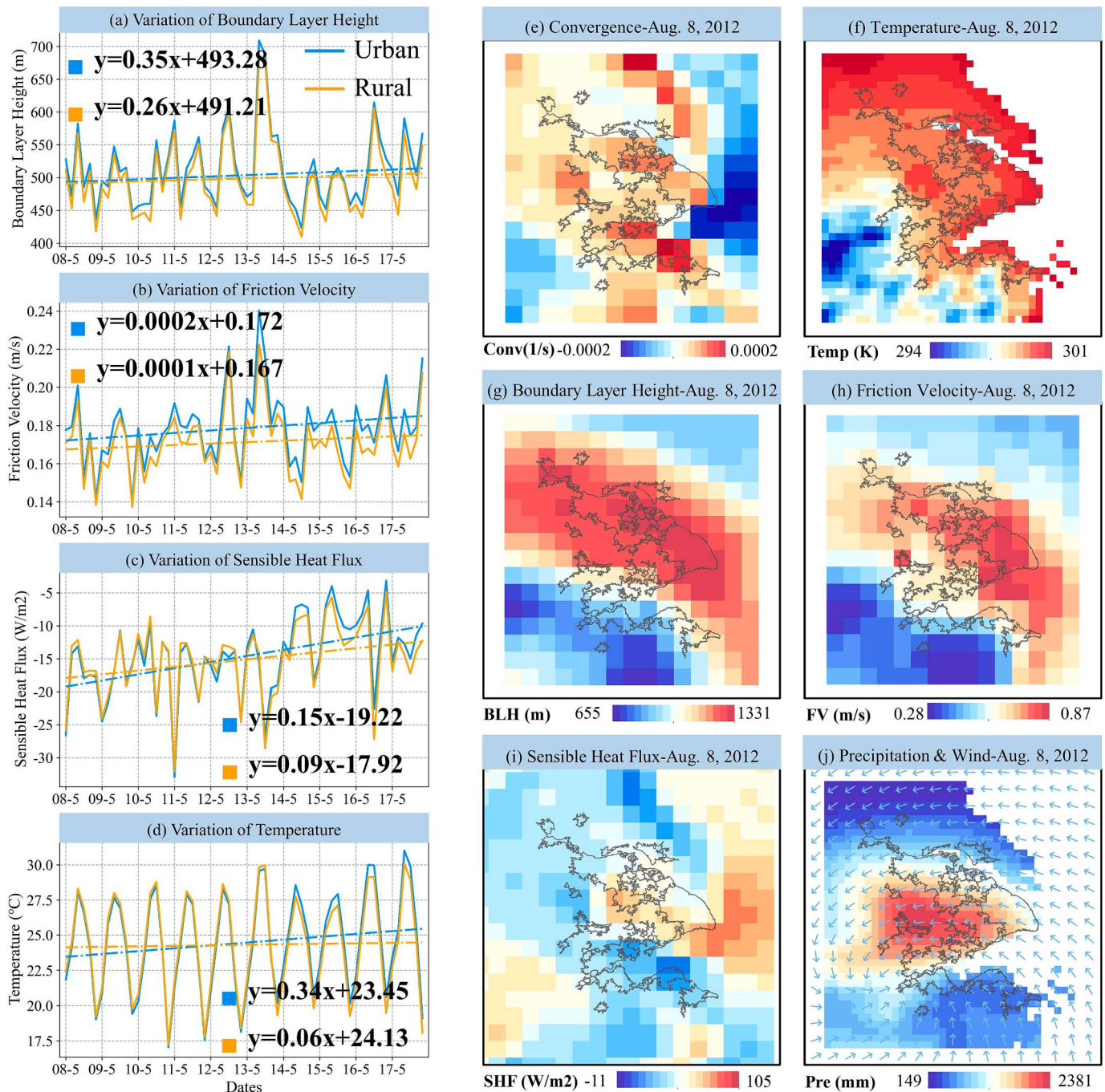


Fig. 11. The potential influencing factors of urbanization effects on runoff. The first column shows the temporal variations of runoff-related factors in urban and rural regions over three urban agglomerations. The second and the third columns represent the spatial distributions of runoff-related factors during August 8, 2012 when the typhoon Haikui landed.

faster and more intensive accumulation of surface runoff under heavy rainfall events. Previous results have confirmed that the vegetated area had relatively lower annual runoff and peak ratio. To this point, the increase of green infrastructure in the urban regions can enhance the infiltration and evapotranspiration of the ground water and further mitigate the increase of surface runoff induced by urbanization (Kim and Park, 2016). In addition, the increase of green space can also potentially reduce the surface roughness, which will weaken the UHI effects associated with the intensive urban rainfall (Debbage and Shepherd, 2019; Debbage and Shepherd, 2018). On the other hand, the results demonstrated that the spatial patterns of surface runoff showed discrepancies in the compact-arranged urban regions and open urban regions.

Rosenberger et al. (2021) concluded that the densification of buildings may have adverse effects on the environment as well as life quality in the urban regions. The findings highlight the importance of the consideration of building arrangement during urban planning to mitigate the stormwater and flooding hazard. In addition, some low impact development (LID) techniques (e.g., rain barrels, infiltration trenches, disconnected green roofs, bio-retention ponds) are promising to cope with the challenges of more intensive rainfall events under urbanization and climate change (Pour et al., 2020; Yang et al., 2022; Wadhwa et al., 2023).

6. Conclusions

Urbanization has become an irreversible trend and recent research has demonstrated that urbanization is even more rapid in flood-prone area. Nevertheless, to what extent does the urbanization affect and contribute to the alteration of channel and surface runoff still lacks quantitative analysis within urban extents with limited availability of data. In this study, we designed a quantitative framework by integrating both physical and empirical hydrological model to address the research gaps.

The model-based simulation in this study revealed that urbanization tended to enhance both channel runoff and surface runoff in three urban agglomerations in YRB. Specifically, the channel runoff increased by 4.4 %, 5 %, and 12.08 % in CY, MRYR, and YRD urban agglomerations, respectively. Like the variation of channel runoff, the urbanization effects on channel runoff also exhibited prominent seasonality, with more significant effects in summer and less significant in spring. In addition, the variation of surface runoff also showed positive relationship with the increment of impervious surface under urbanization. Results of trend analysis demonstrated that urbanization contributed to 30 %, 21.4, and 17.7 % of the surface runoff changes in CY, MRYR, and YRD, respectively. Further case simulations by selecting specific severe flood events and setting the heavy rainfall situation also confirmed the enhancement of channel runoff and surface runoff under urbanization.

By classifying the urban regions according to the building height (e.g., high-rise, middle-rise, low-rise) and arrangement (e.g., compact, open), our results highlighted that the HR, MR, and CP regions were more prone to accumulate surface runoff and trigger flood hazard due to the weaker infiltration capacity of land surface under the densely distribution of impervious surface. Besides, the identification of urban runoff clusters also provided spatial knowledge about the high/low runoff hotspots and the potential regions for runoff mitigation, which is of great significance for the development of urban planning policies.

In addition, we mapped the distributions of various hydro-meteorological factors under a given storm rainfall event to elucidate the potential mechanisms underlying urbanization effects on runoff. Urbanization enhanced the wind convergence and surface roughness, creating favorable condition for rainfall in urban regions. Besides, the urbanization-induced UHI effect and increased sensible heat flux also elevated the atmospheric boundary layer and affected the stability of atmosphere, which contributed to the occurrence of convective precipitation. Overall, the combined effects of the urbanization on local climate and underlying surface enhanced the extreme rainfall. As urban areas are densely distributed with impervious surfaces, it hindered the infiltration of runoff and caused it to flow directly into rivers, ultimately increasing both surface and channel runoff.

The results of this study are expected to provide quantitative evidence about the urbanization induced runoff changes and give implications for prioritizing measures in flood prevention and preparedness, such as the consideration of building arrangement, green infrastructure, and the LID techniques. Moreover, as the data used for model simulation in this study is widely available, the proposed framework can also be applied in other river basins and cities to study the local-scale hydro-meteorological responses to the climate and anthropogenic impacts.

CRediT authorship contribution statement

Shuzhe Huang: Writing – original draft, Methodology, Formal analysis, Conceptualization. **Yuan Gan:** Writing – review & editing, Software, Methodology. **Nengcheng Chen:** Writing – review & editing, Conceptualization, Funding acquisition. **Chao Wang:** Writing – review & editing. **Xiang Zhang:** Writing – original draft. **Chuxuan Li:** Writing – review & editing, Methodology. **Daniel E. Horton:** Writing – review & editing.

Declaration of competing interest

The authors declare that they have no known competing financial interests or personal relationships that could have appeared to influence the work reported in this paper.

Data availability

The MOD13Q1 product can be downloaded at <https://lpdaac.usgs.gov/tools/appeears/>. The GISA2.0 dataset is available at <https://zenodo.org/record/5136330>. The global LCZ map can be accessed at <https://zenodo.org/record/6364594>. The HYSOGs250m product is available at https://daac.ornl.gov/cgi-bin/dsviewer.pl?ds_id=1566. The CMFD dataset can be downloaded at <https://data.tpdc.ac.cn/zh-hans/data/8028b944-daaa-4511-8769-965612652c49>. The HRLT dataset can be downloaded at <https://doi.org/10.1594/PANGAEA.941329>. The ERA5 product can be accessed at <https://www.ecmwf.int/en/forecasts/datasets/reanalysis-datasets/era5>.

Acknowledgement

This work was supported by grants from the National Natural Science Foundation of China program (41890822, 41801339), the Special Fund of Hubei Luojia Laboratory (220100034), the Open Fund of Hubei Luojia Laboratory (220100059), and the Open Fund of National Engineering Research Center for Geographic Information System, China University of Geosciences, Wuhan 430074, China (Grant No. 2022KFJJ07). C.L. and D.E.H. acknowledge support from U.S. National Science Foundation PREEVENTS Award 1848683. The numerical calculations in this paper have been done on the supercomputing system in the Supercomputing Center of Wuhan University.

Appendix A. Supplementary data

Supplementary data to this article can be found online at <https://doi.org/10.1016/j.jhydrol.2024.131194>.

References

- Anand, J., Gosain, A.K., Khosa, R., 2018. Prediction of land use changes based on Land Change Modeler and attribution of changes in the water balance of Ganga basin to land use change using the SWAT model. *Sci. Total Environ.* 644, 503–519. <https://doi.org/10.1016/j.scitotenv.2018.07.017>.
- Bai, L., et al., 2022. Domain adaptation for remote sensing image semantic segmentation: an integrated approach of contrastive learning and adversarial learning. *IEEE Trans. Geosci. Remote Sens.* 60, 1–13. <https://doi.org/10.1109/tgrs.2022.3198972>.
- Bai, L., et al., 2023. Geographic mapping with unsupervised multi-modal representation learning from VHR images and POIs. *ISPRS J. Photogramm. Remote Sens.* 201, 193–208. <https://doi.org/10.1016/j.isprsjprs.2023.05.006>.
- Berezowski, T., Chormański, J., Batelaan, O., Canters, F., Van de Voorde, T., 2012. Impact of remotely sensed land-cover proportions on urban runoff prediction. *Int. J. Appl. Earth Obs. Geoinf.* 16, 54–65. <https://doi.org/10.1016/j.jag.2011.11.007>.
- Bibi, T.S., Kara, K.G., Bedada, H.J., Bededa, R.D., 2023. Application of PCSWMM for assessing the impacts of urbanization and climate changes on the efficiency of stormwater drainage systems in managing urban flooding in Robe town Ethiopia. *Journal of Hydrology: Regional Studies* 45, 101291. <https://doi.org/10.1016/j.ejrh.2022.101291>.
- Biggs, T., Zeigler, A., Taniguchi-Quan, K.T., 2022. Runoff and sediment loads in the Tijuana River: dam effects, extreme events, and change during urbanization. *J. Hydrol.: Reg. Stud.* 42, 101162 <https://doi.org/10.1016/j.ejrh.2022.101162>.
- Chen, D., Jiang, P., Li, M., 2021. Assessing potential ecosystem service dynamics driven by urbanization in the Yangtze River Economic Belt China. *Journal of Environmental Management* 292, 112734. <https://doi.org/10.1016/j.jenvman.2021.112734>.
- Chen, J., Theller, L., Gitau, M.W., Engel, B.A., Harbor, J.M., 2017. Urbanization impacts on surface runoff of the contiguous United States. *J. Environ. Manage.* 187, 470–481. <https://doi.org/10.1016/j.jenvman.2016.11.017>.
- Ching, J., et al., 2018. WUDAPT: an urban weather, climate, and environmental modeling infrastructure for the anthropocene. *Bull. Am. Meteorol. Soc.* 99 (9), 1907–1924. <https://doi.org/10.1175/bams-d-16-0236.1>.
- Debbage, N., Shepherd, J.M., 2018. The Influence of urban development patterns on streamflow characteristics in the charlanta megaregion. *Water Resour. Res.* 54 (5), 3728–3747. <https://doi.org/10.1029/2017wr021594>.

- Debbage, N., Shepherd, J.M., 2019. Urban influences on the spatiotemporal characteristics of runoff and precipitation during the 2009 atlanta flood. *J. Hydrometeorol.* 20 (1), 3–21. <https://doi.org/10.1175/jhm-d-18-0010.1>.
- Demuzere, M., et al., 2022. A global map of local climate zones to support earth system modelling and urban-scale environmental science. *Earth Syst. Sci. Data* 14 (8), 3835–3873. <https://doi.org/10.5194/essd-14-3835-2022>.
- Demuzere, M., Bechtel, B., Mills, G., 2019. Global transferability of local climate zone models. *Urban Clim.* 27, 46–63. <https://doi.org/10.1016/j.ulclim.2018.11.001>.
- Dhar, T., Miglietta, D.M.M., Rawat, D.B.S., 2022. Calibration of WRF hydro for bhagirathi alakananda basin. *International Journal of Engineering and Advanced Technology* 11 (5), 24–29. <https://doi.org/10.35940/ijeat.E3524.0611522>.
- Du, J., et al., 2012. Assessing the effects of urbanization on annual runoff and flood events using an integrated hydrological modeling system for Qinhuai River basin, China. *J. Hydrol.* 464–465, 127–139. <https://doi.org/10.1016/j.jhydrol.2012.06.057>.
- Du, R., Liu, C.-H., Li, X.-X., Lin, C.-Y., 2023. Effect of local climate zone (LCZ) and building category (BC) classification on the simulation of urban climate and air-conditioning load in Hong Kong. *Energy* 271, 127004. <https://doi.org/10.1016/j.energy.2023.127004>.
- Fan, F., Deng, Y., Hu, X., Weng, Q., 2013. Estimating composite curve number using an improved SCS-CN method with remotely sensed variables in Guangzhou China. *Remote Sensing* 5 (3), 1425–1438. <https://doi.org/10.3390/rs5031425>.
- Fang, C., 2015. Important progress and future direction of studies on China's urban agglomerations. *J. Geog. Sci.* 25 (8), 1003–1024. <https://doi.org/10.1007/s11442-015-1216-5>.
- Fang, C., Ma, H., Wang, J., 2015. A regional categorization for “new-type urbanization” in China. *PLoS One* 10 (8), e0134253.
- Gochis, D., et al., 2019. Overview of national water model calibration general strategy & optimization. National Center for Atmospheric Research.
- Guerreiro, S.B., et al., 2018. Detection of continental-scale intensification of hourly rainfall extremes. *Nat. Clim. Chang.* 8 (9), 803–807. <https://doi.org/10.1038/s41558-018-0245-3>.
- Guo, W., Jiao, X., Zhou, H., Zhu, Y., Wang, H., 2022. Hydrologic regime alteration and influence factors in the Jialing River of the Yangtze River China. *Scientific Reports* 12 (1). <https://doi.org/10.1038/s41598-022-15127-4>.
- He, J., et al., 2020. The first high-resolution meteorological forcing dataset for land process studies over China. *Sci. Data* 7 (1), 25. <https://doi.org/10.1038/s41597-020-0369-y>.
- Hu, T., Huang, X., 2019. A novel locally adaptive method for modeling the spatiotemporal dynamics of global electric power consumption based on DMSP-OLS nighttime stable light data. *Appl. Energy* 240, 778–792. <https://doi.org/10.1016/j.apenergy.2019.02.062>.
- Huang, S., et al., 2022a. Urbanization-induced drought modification: example over the Yangtze River Basin. *China. Urban Climate* 44, 101231. <https://doi.org/10.1016/j.ulclim.2022.101231>.
- Huang, X., et al., 2022b. Toward accurate mapping of 30-m time-series global impervious surface area (GISA). *Int. J. Appl. Earth Obs. Geoinf.* 109, 102787 <https://doi.org/10.1016/j.jag.2022.102787>.
- Huang, S., et al., 2023a. Urbanization amplified asymmetrical changes of rainfall and exacerbated drought: analysis over five urban agglomerations in the Yangtze River Basin. *China. Earth's Future* 11 (2). <https://doi.org/10.1029/2022ef003117>.
- Huang, S., Zhang, X., Wang, C., Chen, N., 2023b. Two-step fusion method for generating 1 km seamless multi-layer soil moisture with high accuracy in the Qinghai-Tibet plateau. *ISPRS J. Photogramm. Remote Sens.* 197, 346–363. <https://doi.org/10.1016/j.isprsjprs.2023.02.009>.
- Ke, G., et al., 2017. LightGBM: A Highly Efficient Gradient Boosting Decision Tree. Kendall, M.G., 1948. Rank correlation methods.
- Kilicarslan, B.M., Yucel, I., Pilatlin, H., Duzenli, E., Yilmaz, M.T., 2021. Improving WRF-Hydro runoff simulations of heavy floods through the sea surface temperature fields with higher spatio-temporal resolution. *Hydrol. Process.* 35 (9) <https://doi.org/10.1002/hyp.14338>.
- Kim, H.W., Park, Y., 2016. Urban green infrastructure and local flooding: the impact of landscape patterns on peak runoff in four Texas MSAs. *Appl. Geogr.* 77, 72–81. <https://doi.org/10.1016/j.apgeog.2016.10.008>.
- Kishtawal, C., Niyogi, D., Tewari, M., Pielke Sr, R., Shepherd, M., 2010. Urbanization signature in the observed heavy rainfall climatology over India. *Int. J. Climatol.* 30, 1908–1916. <https://doi.org/10.1002/joc.2044>.
- Kong, D., Gu, X., Li, J., Ren, G., Liu, J., 2020. Contributions of global warming and urbanization to the intensification of human-perceived heatwaves Over China. *J. Geophys. Res. Atmos.* 125 (18) <https://doi.org/10.1029/2019jd032175>.
- Kubal, C., Haase, D., 2009. Integrated urban flood risk assessment - adapting a multicriteria approach to a city. *Nat. Hazards Earth Syst. Sci.* 9 <https://doi.org/10.5194/nhess-9-1881-2009>.
- Li, C., et al., 2018. Effects of urbanization on direct runoff characteristics in urban functional zones. *Sci. Total Environ.* 643, 301–311. <https://doi.org/10.1016/j.scitotenv.2018.06.211>.
- Li, X., et al., 2020. Mapping global urban boundaries from the global artificial impervious area (GAIA) data. *Environ. Res. Lett.* 15 (9), 094044 <https://doi.org/10.1088/1748-9326/ab9be3>.
- Li, C., et al., 2022. Augmentation of WRF-Hydro to simulate overland-flow- and streamflow-generated debris flow susceptibility in burn scars. *Nat. Hazards Earth Syst. Sci.* 22 (7), 2317–2345. <https://doi.org/10.5194/nhess-22-2317-2022>.
- Li, C., et al., 2023a. Runoff variations affected by climate change and human activities in Yarlung Zangbo River, southeastern Tibetan Plateau. *Catena* 230. <https://doi.org/10.1016/j.catena.2023.107184>.
- Li, F., Liu, Y., Engel, B.A., Chen, J., Sun, H., 2019. Green infrastructure practices simulation of the impacts of land use on surface runoff: Case study in Ecorse River watershed, Michigan. *J. Environ. Manage.* 233, 603–611. <https://doi.org/10.1016/j.jenvman.2018.12.078>.
- Li, C., Yu, G., Wang, J., Horton, D., 2023b. Toward Improved Regional Hydrological Model Performance Using a Novel Soil Data-Informed Calibration Method. <https://doi.org/10.22541/essoar.167340706.60948782/v1>.
- Liu, Y., Huang, X., Yang, H., 2022. An integrated approach to investigate the coupling coordination between urbanization and flood disasters in China. *J. Clean. Prod.* 375, 134191 <https://doi.org/10.1016/j.jclepro.2022.134191>.
- Liu, K., Li, X., Wang, S., 2021a. Characterizing the spatiotemporal response of runoff to impervious surface dynamics across three highly urbanized cities in southern China from 2000 to 2017. *Int. J. Appl. Earth Obs. Geoinf.* 100, 102331 <https://doi.org/10.1016/j.jag.2021.102331>.
- Liu, S., Wang, J., Wei, J., Wang, H., 2021b. Hydrological simulation evaluation with WRF-Hydro in a large and highly complicated watershed: The Xijiang River basin. *J. Hydrol.: Reg. Stud.* 38, 100943 <https://doi.org/10.1016/j.ejrh.2021.100943>.
- Lundberg, S., Lee, S.-I., 2017. A Unified Approach to Interpreting Model Predictions. Mann, H.B., 1945. Nonparametric Tests Against Trend. *Econometrica* 13 (3), 245–259. <https://doi.org/10.2307/1907187>.
- Maragno, D., et al., 2018. Fine-scale analysis of urban flooding reduction from green infrastructure: an ecosystem services approach for the management of water flows. *Ecol. Model.* 386, 1–10. <https://doi.org/10.1016/j.ecolmodel.2018.08.002>.
- Miller, J.D., Hess, T., 2017. Urbanisation impacts on storm runoff along a rural-urban gradient. *J. Hydrol.* 552, 474–489. <https://doi.org/10.1016/j.jhydrol.2017.06.025>.
- Pandit, A., Gopalakrishnan, G., 1996. Estimation of annual storm runoff coefficients by continuous simulation. *Journal of Irrigation and Drainage Engineering-ASCE – J. Irrig. Drain Eng.-ASCE* 122. [https://doi.org/10.1061/\(ASCE\)0733-9437\(1996\)122:4\(211\)](https://doi.org/10.1061/(ASCE)0733-9437(1996)122:4(211)).
- Pour, S.H., Wahab, A.K.A., Shahid, S., Asaduzzaman, M., Dewan, A., 2020. Low impact development techniques to mitigate the impacts of climate-change-induced urban floods: current trends, issues and challenges. *Sustain. Cities Soc.* 62 <https://doi.org/10.1016/j.scs.2020.102373>.
- Qin, R., et al., 2022. HRLT: a high-resolution (1 d, 1 km) and long-term (1961–2019) gridded dataset for surface temperature and precipitation across China. *Earth Syst. Sci. Data* 14 (11), 4793–4810. <https://doi.org/10.5194/essd-14-4793-2022>.
- Quenum, G.M.L.D., et al., 2022. Potential of the coupled WRF/WRF-hydro modeling system for flood forecasting in the Ouémé River (West Africa). *Water* 14 (8). <https://doi.org/10.3390/w14081192>.
- Ramezani, M.R., Helffer, F., Yu, B., 2023. Individual and combined impacts of urbanization and climate change on catchment runoff in Southeast Queensland, Australia. *Sci. Total Environ.* 861, 160528 <https://doi.org/10.1016/j.scitotenv.2022.160528>.
- Rosenberger, L., Leandro, J., Pauleit, S., Erlwein, S., 2021. Sustainable stormwater management under the impact of climate change and urban densification. *J. Hydrol.* 596, 126137 <https://doi.org/10.1016/j.jhydrol.2021.126137>.
- Ross, C.W., et al., 2018. HYSGOs250m, global gridded hydrologic soil groups for curve-number-based runoff modeling. *Sci. Data* 5, 180091. <https://doi.org/10.1038/sdata.2018.91>.
- Sathish Kumar, D., Arya, D.S., Vojinovic, Z., 2013. Modeling of urban growth dynamics and its impact on surface runoff characteristics. *Comput. Environ. Urban Syst.* 41, 124–135. <https://doi.org/10.1016/j.compenvurbsys.2013.05.004>.
- Schmitt, T.G., Thomas, M., Ettrich, N., 2004. Analysis and modeling of flooding in urban drainage systems. *J. Hydrol.* 299 (3–4), 300–311. <https://doi.org/10.1016/j.jhydrol.2004.08.012>.
- Schoener, G., 2018. Urban runoff in the U.S. southwest: importance of impervious surfaces for small-storm hydrology. *J. Hydrol. Eng.* 23 (2) [https://doi.org/10.1061/\(ASCE\)HE.1943-5584.0001610](https://doi.org/10.1061/(ASCE)HE.1943-5584.0001610).
- Sen, P., 1968. Estimates of the regression coefficient based on Kendall's Tau. *J. Am. Stat. Assoc.* 63 (324) <https://doi.org/10.1080/01621459.1968.10480934>.
- Seto, K., Güneralp, B., Hutyra, L., 2012. Global forecasts of urban expansion to 2030 and direct impacts on biodiversity and carbon pools. *Proc. Natl. Acad. Sci.* 109, 16083–16088. <https://doi.org/10.1073/pnas.1211658109>.
- Shem, W., Shepherd, M., 2009. On the impact of urbanization on summertime thunderstorms in Atlanta: two numerical model case studies. *Atmos. Res.* 92 (2), 172–189. <https://doi.org/10.1016/j.atmosres.2008.09.013>.
- Shen, P., Zhao, S., Ma, Y., Liu, S., 2023. Urbanization-induced Earth's surface energy alteration and warming: A global spatiotemporal analysis. *Remote Sens. Environ.* 284, 113361 <https://doi.org/10.1016/j.rse.2022.113361>.
- Singh, J., Karmakar, S., PaiMazumder, D., Ghosh, S., Niyogi, D., 2020. Urbanization alters rainfall extremes over the contiguous United States. *Environ. Res. Lett.* 15 (7), 074033 <https://doi.org/10.1088/1748-9326/ab8980>.
- Sofokleous, I., Bruggeman, A., Camera, C., Eliades, M., 2023. Grid-based calibration of the WRF-Hydro with Noah-MP model with improved groundwater and transpiration process equations. *J. Hydrol.* 617, 128991 <https://doi.org/10.1016/j.jhydrol.2022.128991>.
- Sun, Y., et al., 2014. Rapid increase in the risk of extreme summer heat in Eastern China. *Nat. Clim. Chang.* 4 (12), 1082–1085. <https://doi.org/10.1038/nclimate2410>.
- Sun, L., Chen, J., Li, Q., Huang, D., 2020. Dramatic uneven urbanization of large cities throughout the world in recent decades. *Nat. Commun.* 11 (1), 5366. <https://doi.org/10.1038/s41467-020-19158-1>.
- Thielen, J., Wobrock, W., Gadian, A., Mestayer, P., Creutin, J., 2000. The possible influence of urban surfaces on rainfall development: a sensitivity study in 2D in the meso-gamma-scale. *Atmos. Res.* 54, 15–39. [https://doi.org/10.1016/S0169-8095\(00\)00041-7](https://doi.org/10.1016/S0169-8095(00)00041-7).

- Wadhwa, A., Budamala, V., Kummamuru, P.K., Kasiviswanathan, K.S., 2023. Low-impact development (LID) control feasibility in a small-scale urban catchment for altered climate change scenarios. *Hydrol. Sci. J.* 68 (13), 1881–1894. <https://doi.org/10.1080/02626667.2023.2239797>.
- Walker, J.J., Soulard, C.E., Petrakis, R.E., 2020. Integrating stream gage data and Landsat imagery to complete time-series of surface water extents in Central Valley, California. *Int. J. Appl. Earth Obs. Geoinf.* 84, 101973 <https://doi.org/10.1016/j.jag.2019.101973>.
- Wang, W., et al., 2022. A WRF/WRF-Hydro coupling system with an improved structure for rainfall-runoff simulation with mixed runoff generation mechanism. *J. Hydrol.* 612 <https://doi.org/10.1016/j.jhydrol.2022.128049>.
- Wang, J., Feng, J., Yan, Z., 2015. Potential sensitivity of warm season precipitation to urbanization extents: modeling study in Beijing-Tianjin-Hebei urban agglomeration in China. *J. Geophys. Res. Atmos.* 120 (18), 9408–9425. <https://doi.org/10.1002/2015jd023572>.
- Wang, J., Chen, F., Doan, Q.-V., Xu, Y., 2021. Exploring the effect of urbanization on hourly extreme rainfall over Yangtze River Delta of China. *Urban Clim.* 36, 100781 <https://doi.org/10.1016/j.uclim.2021.100781>.
- Wang, S., Zhang, X., Wang, C., Chen, N., 2023. Multivariable integrated risk assessment for cyanobacterial blooms in eutrophic lakes and its spatiotemporal characteristics. *Water Res.* 228 (Pt A), 119367 <https://doi.org/10.1016/j.watres.2022.119367>.
- Westra, S., Brown, C., Lall, U., Sharma, A., 2007. Modeling multivariable hydrological series: principal component analysis or independent component analysis? *Water Resour. Res.* 43 (6) <https://doi.org/10.1029/2006wr005617>.
- Wu, Y., et al., 2022. Evolution of river network due to urbanization in the Southeast Yinzhou Plain of Yongjiang River Basin China. *Journal of Cleaner Production* 379, 134718. <https://doi.org/10.1016/j.jclepro.2022.134718>.
- Xiang, T., Vivoni, E.R., Gochis, D.J., Mascaro, G., 2017. On the diurnal cycle of surface energy fluxes in the North American monsoon region using the WRF-Hydro modeling system. *J. Geophys. Res. Atmos.* 122 (17), 9024–9049. <https://doi.org/10.1002/2017jd026472>.
- Xu, C., et al., 2020. Surface runoff in urban areas: the role of residential cover and urban growth form. *J. Clean. Prod.* 262, 121421 <https://doi.org/10.1016/j.jclepro.2020.121421>.
- Xu, C., Haase, D., Pauleit, S., 2018. The impact of different urban dynamics on green space availability: a multiple scenario modeling approach for the region of Munich, Germany. *Ecol. Ind.* 93, 1–12. <https://doi.org/10.1016/j.ecolind.2018.04.058>.
- Yang, P., Ren, G., Yan, P., Deng, J., 2021. Urbanization reduces frequency of light rain: an example from Beijing City. *Theor. Appl. Climatol.* 145 (1–2), 763–774. <https://doi.org/10.1007/s00704-021-03655-4>.
- Yang, L., Smith, J., Niyogi, D., 2019. Urban impacts on extreme monsoon rainfall and flooding in complex terrain. *Geophys. Res. Lett.* 46 <https://doi.org/10.1029/2019GL083363>.
- Yang, W., Zhang, J., Krebs, P., 2022. Low impact development practices mitigate urban flooding and non-point pollution under climate change. *J. Clean. Prod.* 347 <https://doi.org/10.1016/j.jclepro.2022.131320>.
- Yao, L., Chen, L., Wei, W., Sun, R., 2015. Potential reduction in urban runoff by green spaces in Beijing: a scenario analysis. *Urban For. Urban Green.* 14 (2), 300–308. <https://doi.org/10.1016/j.ufug.2015.02.014>.
- Yu, X., et al., 2022. Asymmetrical shift toward less light and more heavy precipitation in an urban agglomeration of East China: intensification by urbanization. *Geophys. Res. Lett.* 49 (4) <https://doi.org/10.1029/2021gl097046>.
- Yuan, Y., Cave, M., Zhang, C., 2018. Using Local Moran's I to identify contamination hotspots of rare earth elements in urban soils of London. *Appl. Geochem.* 88, 167–178. <https://doi.org/10.1016/j.apgeochem.2017.07.011>.
- Yucel, I., Onen, A., Yilmaz, K.K., Gochis, D.J., 2015. Calibration and evaluation of a flood forecasting system: Utility of numerical weather prediction model, data assimilation and satellite-based rainfall. *J. Hydrol.* 523, 49–66. <https://doi.org/10.1016/j.jhydrol.2015.01.042>.
- Zhang, X., et al., 2021. The temporal variations in runoff-generation parameters of the Xinanjiang model due to human activities: a case study in the upper Yangtze River Basin China. *Journal of Hydrology: Regional Studies* 37. <https://doi.org/10.1016/j.ejrh.2021.100910>.
- Zhang, L., et al., 2022. Direct and indirect impacts of urbanization on vegetation growth across the world's cities. *Sci. Adv.* 8 <https://doi.org/10.1126/sciadv.abo0095>.
- Zhang, W., Villarini, G., Vecchi, G.A., Smith, J.A., 2018b. Urbanization exacerbated the rainfall and flooding caused by hurricane Harvey in Houston. *Nature* 563 (7731), 384–388. <https://doi.org/10.1038/s41586-018-0676-z>.
- Zhang, L., Zhang, M., Yao, Y., 2018a. Mapping seasonal impervious surface dynamics in Wuhan urban agglomeration, China from 2000 to 2016. *Int. J. Appl. Earth Obs. Geoinf.* 70, 51–61. <https://doi.org/10.1016/j.jag.2018.04.005>.
- Zheng, Y., et al., 2023. Mapping the spatial distribution of nocturnal urban heat island based on Local Climate Zone framework. *Build. Environ.* 234, 110197 <https://doi.org/10.1016/j.buildenv.2023.110197>.